Chapter 1: Introduction

1.1 Transition metal carbides

Transition metal carbides have many achievable applications due to their special properties, such as extreme hardness, extremely high melting points, excellent high-temperature strength, good corrosion resistance, excellent electric and thermal conductivity. For example, they can be used in rocket nozzles, drill bits, coatings for cutting and milling tools and inserts, nuclear-fission power plants and thermal spray powder.[1-4] Table 1-1 lists some physical properties of transition metal carbides.[3] Many transition metal carbides also show interesting catalytic behavior, such as hydrogenation, hydrogenolysis, isomerization, hydrodesulfurization and hydrodenitrogenation of hydrocarbons.[2]

Table 1-1 Some physical properties of transition metal carbides

Materials	Vickers Hardness (GPa)	Melting Point (℃)	Electrical Resistivity at 20 ℃ ($\mu \Omega \cdot$cm)	Thermal Conductivity at 20 ℃ (W/m•K)
TiC	28-35	3067	68	21.0
ZrC	25.9	3420	43	20.5
HfC	26.1	3928	37	20.0
VC	27.2	2830	60	38.9
NbC	19.6	3600	35	14.2
TaC	16.7	3950	25	22.1
Cr_3C_2	10-18	1810	75	19
Mo_2C	15.5-24.5	2520	71	21.5
WC	22	2870	22	63

1.2 Transition metal oxides

The transition metal oxides offer a wide variety of important physical and electronic properties, including magnetism, superconductivity, ferroelectricity, nonlinear optical behavior, ionic conductivity.[5-7] They are good insulators, semiconductors, metals and superconductors. Table 1-2 lists some properties of transition metal oxides. Many transition

1

metal oxides also show catalytic properties, such as hydrogenation, dehydrogenation, isomerization, decomposition of alcohols.[6]

Table 1-2 Some transition metal oxides and their properties

Paramagnetism	Superconductivity	Ferroelectricity	Nonlinear optics	Ionic conductivity
Ti_2O_3	$La_{2-x}Ba_xCuO_{4-x}$	$BaTiO_3$	$LiNbO_3$	ZrO_2
VO	$YBa_2Cu_3O_7$	$KNaC_4H_4O_6 \cdot 4H_2O$	$KTiO(PO_4)$	Y_2O_3
VO_2		$KNbO_3$		
NdO_2		$LiNbO_3$		
		$PbTiO_3$		

1.3 The properties of group VI metal carbides

The physical properties of group VI carbides are similar since they have similar atomic bonding, composition and crystal structures. Table 1-3 lists the crystal properties of these three carbides.[8]

Table 1-3 The crystal properties of group VI metal carbides

Materials	Phase	Crystal structure and lattice parameters (Å)	Space group
Chromium carbide	Cr_7C_3	Hexagonal, a = 13.98, c = 4.523	P31c
	Cr_3C_2	Orthorhombic, a = 11.46, b = 5.52, c = 2.821	Pbnm
	$Cr_{23}C_6$	Cubic, a = 10.63	Fm3m
Molybdenum carbide	β-Mo_2C	Hexagonl, a = 3.012, c = 4.735	$P6_{3/mmc}$
	α-Mo_2C	Orthorhombic, a = 4.732, b = 6.037, c = 5.204	Pbcn
	MoC_{1-x}	Hexagonl, a = 2.932, c = 10.970	$P6_{3/mmc}$
		Cubic, a = 4.273	Fm3m
	W_2C	Hexagonal, a = 2.99, c = 4.72	P3m1
Tungsten carbide	WC	Hexagonal, a = 2.91, c = 2.84	P6m2
	WC_{1-x}	Cubic, a = 4.235	Fm3m

In particular, the catalytic properties of carbides of group VI are excellent in these carbides because of their availability in high surface area form with reasonably clean surfaces for many reactions such as hydrogenation, hydrogenolysis, isomerization,

hydrodesulfurzation (HDS) and hydrodenitrogenation (HDN) of hydrocarbon. For example, molybdenum carbide and β-W_2C are comparable to the best group 8 − 10 metals (Ni, Pd and Pt) in hydrogenation at the same condition.[9]

1.4 The properties of lithiated oxides of group V and VI metals

In all lithiated oxides of group V, $LiNbO_3$ and $LiTaO_3$ attract our attention to us because of their excellent properties. The properties of $LiNbO_3$ and $LiTaO_3$ include ferroelectric, piezoelectric, optoelectronic and nonlinear optical properties. $LiNbO_3$ and $LiTaO_3$ are very promising materials for surface acoustic wave (SAW) devices, second harmonic generators, optical switches and modulators.[5,10] In lithiated oxides of group VI, Li_xMoO_2 have been identified as a lithium insertion material for the cathode in rechargeable batteries. The theoretical specific capacity of Li_xMoO_2 corresponds to 199 mA h/g.[11] Table 1-4 lists the crystal properties of these three lithiated oxides.[8]

Table 1-4 Structure and lattice parameters of $LiNbO_3$, $LiTaO_3$ and Li_xMoO_2

Materials	Crystal structure	Lattice parameters	Space group
$LiNbO_3$	Hexagonal (rhombohedral)	a = 5.149, c = 13.862	R3c
$LiTaO_3$	Hexagonal (rhombohedral)	a = 5.153, c = 13.755	R3c
Li_xMoO_2	Hexagonal (rhombohedral)	a = 2.866, c = 15.469	R3m

1.5 Solution-phase precursors for synthesis of carbides and lithiated oxides of group V and VI metals

The preparation of nanophase materials has been the focus of intense study in materials science. Homogenous solution-phase precursors have been used to form nanometer-sized carbides of group V and VI at temperature significantly lower than those employed in the traditional methods.[12] Previously, we reported that the synthesis of V_4C_3, NbC and TaC via chemical reduction methods is carried out by mixing metal chloride, VCl_3, $NbCl_5$ and $TaCl_5$,

with n-butyllithium in hexane to generate colloidal powders.[13] These powders were subsequently heat treated at 873－1273 K to produce the carbides of group V. Also, the carbides of group VI, including Cr_2C, Mo_2C and W_2C, were synthesized from the colloid generated by metal chlorides, $CrCl_3$, $MoCl_4(THF)_2$, $MoCl_3(THF)_2$ and WCl_4, respectively, with $LiBEt_3H$ in THF.[14] Recently, sonochemical synthesis of Mo_2C nanoparticles from $Mo(CO)_6$ in liquid phase is a new process.[15]

The preparations of high surface area lithiated oxides of group V and VI in solution routes include polymerized complex methods, evaporative methods and coprecipitation methods. A modified Pechini-type polymerized complex (PC) route based on polyesterification between citric acid (CA) and ethylene glycol (EG) has been successfully used to synthesize LiTaO3 at 773－873 K without any special care about mosture in air.[16-19] $LiNbO_3$ was synthesized from the evaporation of a solution containing an organic niobium soluble salt, ammonium dihydrogen tris(oxalato)oxoniobate(V) trihydrate, lithium nitrate, oxalic acid and ammonium hydroxide.[19] $LiTaO_3$ was prepared from the precipitate generated by tantalum(V) oxide, lithium nitrate, ammonium carbonate and standard ammonia solution.[21] The reaction between MoO(OH) and Li_2CO_3 at 873 K leads to the layered compound $LiMoO_2$.[22]

1.6 The reaction of metal or metal compounds with gas-phase reagents for synthesis of carbides of group VI metals

Another direct method of preparation of carbides is the reaction of metals or metal compounds with gas-phase reagents. The compound can be a metal hydride, oxide, or halide, and is generally a solid. The complete carbonization of metals or metal compounds of group VI is applied at a relatively low temperature. For example, high temperature reduction of $MoCl_5$ by a mixture of 20% of CH_4 in H_2 produced Mo_2C.[23] Reduction of MoO_3 powders by carbon black at high temperatures generated Mo_2C also.[24] Similar reaction methodology was

employed to prepare activated carbon supported bimetallic carbide of molybdenum and tungsten.[25] High-surface-area molybdenum and tungsten carbide materials were synthesised by temperature programming reduction of the relevant metal oxide with methane/hydrogen.[26]

1.7 The purpose of the thesis

The purpose of this study is to prepare the powders of carbides and lithiated oxides of group V and VI from the solution routes and the reactions between the metal and chloroalkane. Chapters 2－4 report the solution-phase routes and Chapters 5－6 belong to solid-gas reactions. Chapter 2 illustrates the activation of THF by alkyllithium reagents to induce the synthesis of nanosized $LiTaO_3$ ($50-100$ nm) and $LiNbO_3$ ($20-50$ nm) powders. Similarly, Li_xMoO_2 powders can be synthesized from the reaction between EtLi and $MoCl_5$ in THF for a long oxidation time. The details are described in Chapter 3. In Chapter 4, several new methods employing colloidal precursors prepared in solutions to synthesize molybdenum carbide particles are reported. In gas-solid reaction, $Mo_2C@a$-C powders have been synthesized from the reactions between Mo metal powders with 1-chlorobutane or with hexachlorobenzene at $873-1173$ K. Carbon hollow spheres ($1-3$ μm) and particles ($200-300$ nm) have been synthesized from CCl_4 and Mo particles template ($1-3$ μm) at 873 K and 1173 K. Two complete presentations of these reactions are well displayed in Chapter 5 and 6, respectively.

1.8 Reference

(1)   Toth, L. E. *Transition Metal Carbides and Nitrides*; Academic Press: New York, 1971.

(2)   Oyama, S. T. *The Chemistry of Transition Metal Carbides and Nitrides*; Blackie

Academic and Professional: Glasgow, 1996.

(3)   Pierson, H. O. *Handbook of Refractory Carbides and Nitrides*; Noyes Publications:

Westwood, 1996.

(4)   Paul, S.; Richard, K. *Refractory Hard Metals*, The Macmillan Company: New York,

1953.

(5)   Cox, P. A.   *Transition Metal Oxide*; Clarendon Press: Oxford, 1992.

(6)   Kung, H. H. *Transition Metal Oxide: Surface Chemistry and Catalysis*; Elsevier Science

Publishing Company: New York, 1989.

(7)   West, A. R. *Basic Solid State Chemistry*; John Wiley & Sons: England, 1999.

(8)   JCPDS: International Center for Diffraction Data, 1601 Park Lane, Swarthmore, PA

19081.

(9)   Hwu, H. H.; Chen, J. G. *Chem. Rev.* **2005**, *105*, 185.

(10) Prokhorov, A. M.; Kuz'minov, Y. S. *Physics and Chemistry of Crystalline Lithium

Niobate*; Adam Hilger: Bristol and New York, 1990.

(11) Barker, J.; Saidi, M. Y.; Swoyer, J. L. *Solid State Ionics* **2003,** *158*, 261.

(12) Wang, L. Z. Characterization of Nanophase Materials; WILEY-VCH Verlag GmbH:

Weinheim, 2000.

(13) Chang, Y.-H.; Chiu, C.-W.; Chen, Y.-C.; Wu, C.-C.; Tsai, C.-P.; Wang J.-L.; Chiu, H.-T. *J.

Mater. Chem.* **2002**, *12*, 2189.

(14) Zeng, D.; Hampden-Smith, M. J. *Chem. Mater.* **1992**, *4*, 968.

(15) Hyeon, T.; Fang, M.; Suslick, K. S. *J. Am. Chem. Soc.* **1996**, *118*, 5492.

(16) Szanics, J.; Okubo, T.; Kakihana, M. *J. Alloys Compd.* **1998**, *281*, 206.

(17) Szanics, J.; Kakihana, M. *Chem. Mater.* **1999**, *11*, 2760.

(18) Camargo, E. R.; Kakihana, M. *Chem. Mater.* **2001**, *13*, 1905.

(19) Camargo, E. R.; Popa, M.; Kakihana, M. *Chem. Mater.* **2002**, *14*, 2365.

(20) Lanfredi, S.; Folgueras-Dominguez-Dominguez S.; Rodrigues A. C. M. *J. Mater. Chem.* **1995**, *5*, 1957.

(21) Navale S.C.; Gaikwad A.B.; Ravi V. *Mater. Lett.* **2006**, *60*, 1047.

(22) Hollingshead J. A.; Tyszkiewicz M. T.; McCarley R. E. *Chem. Mater.* **1993**, *5*, 1600.

(23) Monteverdi, S.; Mercy, M.; Molina, S.; Bettahar, M.M.; Puricelli, S.; Bégin, D.; Maréche, F.; Furdin, F. *Appl. Catal.* **2002,** *230*, 99.

(24) Chaudhury, S.; Mukerjee, S.K.; Vaidya, V.N.; Venugopal, V. *J. Alloys Compd.* **1997,** *261*, 105.

(25) Nguyen, T.H.; Nguyen, T.V.; Lee, Y.J.; Safinski, T.; Adesina, A.A. *Mater. Res. Bull.* **2005,** *40*, 149.

(26) Claridge, J. B.; York, A. P. E.; Brungs, A. J.; Marquez-Alvarez, C.; Sloan, J.; Tsang, S. C.; Green, M. L. H. *J. catal.* **1998**, *180*, 85.

Chapter 2: Tetrahydrofuran Activation Assisted Synthesis of Nanosized Lithium Niobate and Lithium Tantalate

2.1 Introduction

Lithium niobate and lithium tantalate, $LiNbO_3$ and $LiTaO_3$, are perovskite-type, ferroelectric and nonlinear optical materials with many potential applications for surface acoustic wave devices, waveguides in integrated optics, and infrared sensors.[1-4] Low temperature and nano-structural processing of the material are under intensive investigation in recent years. These include a wide range of methods such as polymerized complex (PC) and hydrothermal routes.[5-11] Among these, the PC methods need complicated processing procedures. The hydrothermal method, on the other hand, can only be carried out under high pressure inside high-pressure autoclaves. There are other preparation methods, such as chemical solution techniques. A recent study reported the preparation of related $NaTaO_3$ nanorods from $TaCl_5$ and an alkalide, $K^+(15\text{-crown-5})_2Na^-$ in a THF solution.[12] Nonetheless, the nanorod formation was not easy to control in the reported process.

Previously, we reported a method to synthesize nano-sized early transition metal carbides from colloidal precursors generated by reducing metal chlorides with n-butyllithium in hexane.[13] In this study, we report that by only changing the solvent used in the reaction from hexane to tetrahydrofuran (THF), precursors to nano-sized powders of $LiNbO_3$ and $LiTaO_3$ can be prepared in very simple reaction steps. Apparently, THF can be activated by the alkyllithium reagents, EtLi and ^{n}BuLi, and act as an oxygen source to form the colloidal precursors. With proper adjustment of the ratio of the reactants, followed by heat treatment, the desired compositions of lithium niobate and lithium tantalate are synthesized.

2.2 Experimental Section

2.2.1 General Procedures

Except where it is noted, air and moisture free environment was maintained through the experiment. $NbCl_5$ and $TaCl_5$ were purchased from STREM and used without purification. ^nBuLi and THF were supplied by Aldrich. EtLi was synthesized by reacting EtBr and Li in pentane and sublimed before use. Examples of the $LiMO_3$ preparation steps are listed below.

2.2.2 Instrumentation

X-ray diffraction (XRD) studies were carried out using a MAC MXP-18 diffractometer with Cu Kα radiation. Scanning electron microscopic (SEM) and energy dispersive spectra (EDS) data were collected using a JEOL JSM-6330F at 15 kV. Transmission electron microscopic (TEM) and electron diffraction (ED) images were obtained on a Philips TECNAI 20. X-ray photoelectron spectroscopy (XPS) measurements were carried out using a Perkin-Elmer PHI-1600 spectrometer (Mg Kα at 1253.6 eV, binding energy (B.E.) reference to In $3d_{5/2}$ electron at 443.8 eV, Ar^+ ions as sputtering source at 5 kV, 25 mA). Fourier transform infrared (FT-IR) spectra were recorded using a Nicolet Avatar 360. Raman spectra were measured by using a Jabin Yvon HR800 equipped with a He^+ laser (632.8 nm).

2.2.3 Synthesis of $LiTaO_3$ from precursor formed from $TaCl_5$ and ^nBuLi in THF

To $TaCl_5$ (3.8 g, 11 mmol) dissolved in THF (50 mL), ^nBuLi (23 mL, 2.8 M, 63 mmol) was added to form an air-sensitive black precipitate. After the solvent was removed in vacuum, a black solid was isolated. Then, the solid was heated at 673 K under vacuum for 1 h to form a gray powder. (2.1 g, 81 % yield based on $TaCl_5$)

2.2.4 Synthesis of $LiTaO_3$ from precursor formed from $TaCl_5$ and EtLi in THF

To $TaCl_5$ (1.0 g, 2.8 mmol) dissolved in THF (50 mL), EtLi (0.60 g, 17 mmol) was added. The reaction mixture was stirred under nitrogen for 2 h. Then, it was exposed to air and stirred for 4 h more. The solvent was removed under vacuum to generate a black solid. The solid was heated at 973 K under vacuum for 1 h to give a gray powder. (0.47 g, 71 % yield based on $TaCl_5$)

2.2.5 Synthesis of LiNbO₃ from precursor formed from NbCl₅ and EtLi in THF

To NbCl₅ (1.0 g, 3.7 mmol) dissolved in THF (50 mL), EtLi (0.53 g, 15 mmol) was added. The reaction mixture was stirred under nitrogen for 2 h first. Then, it was stirred for 48 h more in air. After the solvent was removed under vacuum, a black solid was separated. Heating the solid at 873 K under vacuum for 1 h offered a gray powder. (0.25 g, 47 % yield based on NbCl₅)

2.3 Results and Discussion

In general, the reactions between MCl_5 (M = Nb and Ta) and alkyllthiums, ^nBuLi and EtLi, in THF generated dark colloidal solutions. In the cases of using $TaCl_5$, 6 eq of alkyllithiums were needed while in the example of $NbCl_5$ only 4-5 eq of EtLi was introduced. The difference will be further discussed below. For the colloids obtained from the reactions using EtLi, especially in the one employing $NbCl_5$, they were further exposed to air before the heat treatment for a more complete oxidation. In all reactions, the colloids were collected and heat-treated at 673 – 973 K to offer gray solid products in good to excellent yields. When inadequate or excess amount of the alkyllithium reagents were used, the final products were either Li deficient or excess.

Fig. 2-1 shows the representative SEM and TEM images of the powders from $TaCl_5$ and alkyllithiums, ^nBuLi and EtLi, in THF after processed at 773 – 973 K. The SEM and EDS of the sample produced at 873 K, Fig. 2-1(a), displays fine and uniform particle morphology with an average size of about 50 nm. EDS shows the presence of Ta and O in the sample. TEM and ED images of the sample processed at 773 K are shown in Fig. 2-1(b). They also display a homogeneous particle shape with the sizes varied between 40 and 60 nm. The lattice parameters estimated from the ED pattern is consistent with the diffraction of polycrystalline rhombohedral $LiTaO_3$.[14] TEM and ED images of the sample processed at 973 K are shown in Fig. 2-1(c). The size of the particles is larger than that of the samples mentioned above.

Apparently, the particle size enlargement was the consequence of the increased heat treatment temperature. The ED pattern in Fig. 2-1(c) suggests that the sample is crystalline. The derived lattice parameters are consistent with the data of rhombohedral $LiTaO_3$ also. TEM images of the products obtained from the reactions between $NbCl_5$ and EtLi in THF followed by heat-treatment at 873 K are shown in Fig. 2-2. Fig. 2-2(a) displays that the microstructure of the powders is fine particles with uniform sizes 20 – 50 nm. The lattice parameters derived from the ED pattern are consistent with those of the rhombohedral $LiNbO_3$.[15] Fig. 2-2(b) shows the HRTEM image of a particle. The d-spacing measured directly from fringes in the image, 0.37 – 0.38 nm, is close to the interlayer distances of (012) planes estimated from the literature data, 0.375 nm.[15]

The heat treatment temperature affects the product formation significantly. When a low temperature of 573 K was employed, the XRD pattern could only be indexed to the byproduct $LiCl$.[16,17] No reflections could be assigned to Ta containing crystals, such as tantalates. But when a temperature of 673 – 973 K was employed, the XRD patterns of the products were consistent with the pattern of rhombohedral $LiTaO_3$ reported in the literature.[14] For example, the XRD pattern of a sample prepared from $TaCl_5$ and ^nBuLi in THF followed by heat treatment at 773 K is shown in Fig. 2-3(a). No other tantalate phases, such as Ta_2O_5 or Li_3TaO_4, were detected in the sample. The XRD result is consistent with the ED data shown in Fig. 2-1. The other inorganic product, LiCl, was presumably evaporated in the heat treatment process under vacuum. The XRD pattern of a powder prepared from $NbCl_5$ and EtLi in THF followed by heat treatment at 773 K is shown in Fig. 2-3(b). All the reflections can be indexed to rhombohedral $LiNbO_3$ structure reported in the literature.[15]

The survey XPS spectrum of a sample prepared from $TaCl_5$ and ^nBuLi in THF followed by heat treatment at 973 K showed photoelectron signals of Ta, O and C (weak). No signal of Cl was found. A very weak b.e. (binding energy) signal could be seen after a perusal of detailed scans at 56 eV. This was assigned to Li due to its low XPS sensitivity.[18] In the

high-resolution spectrum Fig. 2-4(a), two peaks at b.e. of 28.9 and 27.2 eV are assigned to Ta $4f_{5/2}$ and Ta $4f_{7/2}$ electrons, respectively, in a high oxidation state environment.[18] The shoulder at 23 eV is assigned to the O 2s electron. In Fig. 2-4(b), a strong peak at 531.4 eV is assigned to the O 1s electron in a metal oxide environment. The survey XPS spectrum of a powder prepared from $NbCl_5$ and EtLi in THF followed by heat treatment at 773 K showed the presence of Li, Nb, O and a trace of C. In the high-resolution spectrum Fig. 2-5(a), a very weak signal at 56 eV is assigned to the b.e. of Li 1s electron. Two peaks at b.e. of 210.8 and 208.1 eV, as shown in Fig. 2-5(b), are assigned to the high oxidation state Nb $3d_{3/2}$ and Nb $3d_{5/2}$ electrons, respectively.[19] A strong peak at 531.3 eV in Fig. 2-5(c) is assigned to the O 1s electron in a metal oxide environment.

Raman studies also support the formation of $LiTaO_3$ and $LiNbO_3$ from the precursors processed at high temperatures. Fig. 2-6(a) shows the spectrum of a sample prepared from $TaCl_5$ and EtLi in THF followed by heat treatment at 973 K. It displays typical Raman bands of crystalline $LiTaO_3$.[19] It does not exhibit any significant scattering between 1300 and 1700 cm^{-1}, suggesting that the specimen is virtually free of carbon. Fig. 2-6(b) shows an example prepared by reacting $NbCl_5$ with 4 eq of EtLi and heat-treated at 873 K. The Raman result also agrees with the formation of $LiNbO_3$.[20] The signals from carbon contamination at ca. 1300 and 1600 cm^{-1} were reduced in the samples treated at increased temperatures.

Our previous study showed that ^nBuLi can be used to reduce early transition metal chlorides, such as $NbCl_5$ and $TaCl_5$, in hexane to form colloid precursors for metal carbides.[13] In this study, we simply switched the solvent from hexane to THF and discovered that the colloids formed from $NbCl_5$ and $TaCl_5$ were excellent precursor for $LiNbO_3$ and $LiTaO_3$. Clearly, the solvent THF involved and played an important role in the reaction. As reported in literature, ^nBuLi reacts with THF to form α-lithiotetrahydrofuran. This intermediate probably leads to the cleavage of THF to butane, ethylene, and lithium enolate of acetaldehyde.[21] Except lithium enolate, which appears to be nonvolatile, THF, ethylene and butane were

detected by GC-MS in our study. Thus, we propose that MCl_5 (M = Ta, Nb) reacted with lithium enolate of acetaldehyde, α-lithiotetrahydrofuran, and any residual ^nBuLi in the mixture to generate a colloidal precursor. The precursor is proposed to be a mixture of polymeric Li and M (M = Ta, Nb) alkoxides and the byproduct LiCl. A general reaction pathway is summarized in Scheme 1. IR studies of the precursors indicated the presence of vibrations from M-O, C=C, O-H and THF fragments. Based on the results from GC-MS studies, heating the precursor at 673 K generated many volatile byproducts of saturated and unsaturated C_3-C_8 hydrocarbons.

Controlling the ratio of MCl_5 to the alkyllithiums is important to the successful formation of the $LiMO_3$ precursors in the reactions. The stoichiometry relation between the metalchloride and the alkyllithium is different for the synthesis of $LiNbO_3$ and $LiTaO_3$. In a series of precursor preparations, the ratios of $TaCl_5$ to EtLi were varied from 1:1 to 1:8. Then, the precursors were heated at 973 K and the product phases were studied by XRD. In a Li deficient experiment, with only 1:1 ratio of $TaCl_5$ to EtLi was employed, Ta_2O_5 was the major product, as indicated by the XRD pattern in Fig. 2-7(a).[22] Fig. 2-7(b) shows a product of a mixture of Ta_2O_5 and $LiTaO_3$, the result from a precursor of 1:5 ratio of $TaCl_5$ and EtLi. As the amount of EtLi was increased to 6 eq in the precursor preparation, $LiTaO_3$ was found to be the sole product after the heat treatment, as shown in the XRD in Fig. 2-7(c). Employing 8 eq of EtLi in the reaction resulted in the final formation of Li_3TaO_4, as shown in Fig. 2-7(d).[23] The above information agrees with the simple metathetic pathway suggested in Scheme 2-1. It is suggested that in the reaction, displacements between Ta-Cl bonds and Li-OR bonds lead to the formation of Ta-OR bonds in the polymeric $[LiTa(OR)_m]_n$ precursor. In contrast, heating the precursor from the reaction employing an 1:1 ratio of $NbCl_5$ to EtLi at 873 K, a mixture of NbO_2, $LiNb_3O_8$ and a small amount of $LiNbO_3$ was observed as the product by XRD. The pattern is shown in Fig. 2-8(a).[24,25] The formation of both Nb(IV) and Nb(V) oxides, NbO_2 and lithiated $LiNb_3O_8$, suggests that a reduction of the Nb(V) centers

probably paralleled the metathetic reaction steps. The reduction probably was caused by a homolytic M-L bond cleavage process. This was observed in the synthesis of other Nb complexes before.[26] A beta hydrogen elimination process, from alkylated Nb centers, would be a possible reduction pathway also. The best result for the formation of $LiNbO_3$, showing in Fig. 2-8(b), was from a precursor synthesized by mixing $NbCl_5$ with 4 eq of EtLi followed by exposure to air. The air oxidation probably brought the reduced Nb centers back to the highest oxidation state. Figs. 2-8(c) and 2-8(d) suggest that increasing EtLi from 4 to 6 eq in the precursor preparation resulted in the formation of Li_3NbO_4, in addition to $LiNbO_3$, in significant quantity.[27] The above observations suggest that the precursor formation from $NbCl_5$ was more complex than from $TaCl_5$.

2.4 Conclusion

Nanosized $LiTaO_3$ (50 – 100 nm) and $LiNbO_3$ (20 – 50 nm) powders can be obtained in a simple process. In this, $LiTaO_3$ and $LiNbO_3$ precursors are synthesized by reacting MCl_5 (M = Ta, Nb) with alkyllithiums in THF. Heating the precursors at temperatures 673 – 973 K generates the final solid product. While the process is highly dependent on the reactant ratios and the heat-treatment temperature, the key step to the success of this simple reaction route appears to be the activation of THF by alkyllithium reagents. This enables direct M-O bond formation after a metathetic reaction between M-Cl and Li-OR bonds and facilitates elemental mixing at molecular level in the precursors. This leads to the ultimate formation of $LiTaO_3$ and $LiNbO_3$ at low temperatures.

2.5 References

(1) Cox, P. A. *Transition Metal Oxide*, Clarendon Press: Oxford, **1992**.

(2) Xie, H.; Hsu, W.-Y.; Raj, R. *J. Appl. Phys.* **1995**, *77*, 3420.

(3) Prudkovskiǐ, P. A.; Skugarevkiǐ O. V.; Penin A. N. *J. Exp. Thero. Phys.* **1997**, *85*, 812.

(4) Holm, A.; Stürzer, Q.; Xu, Y.; Weigel, R. *Microelectron. Eng.* **1996**, *31*, 123.

(5) Szanics, J.; Okubo, T.; Kakihana, M. *J. Alloys Compd.* **1998**, *281*, 206.

(6) Szanics, J.; Kakihana, M. *Chem. Mater.* **1999**, *11*, 2760.

(7) Camargo, E. R.; Kakihana, M. *Chem. Mater.* **2001**, *13*, 1905.

(8) Camargo, E. R.; Popa, M.; Kakihana, M. *Chem. Mater.* **2002**, *14*, 2365.

(9) An, C.; Tang, K.; Wang, C.; Shen, G.; Jin, Y.; Qian, Y. *Mater. Res. Bull.* **2002**, *37*, 1791.

(10) Santos, I. C. M. S.; Loureiro, L. H.; Silva, M. F. P.; Cavaleiro, A. M. V. *Polyhedron* **2002**, *21*, 2009.

(11) Niederberger, M.; Pinna, N.; Polleux, J.; Antonietti, M. *Angew. Chem. Int. Ed.* **2004**, *43*, 2270.

(12) Nelsson, J. A.; Wagner, M. J. *J. Am. Chem. Soc.* **2003**, *125*, 332.

(13) Chang, Y.-H.; Chiu, C.-W.; Chen, Y.-C.; Wu, C.-C.; Tsai, C.-P.; Wang, J.-L.; Chiu, H.-T. *J. Mater. Chem.* **2002**, *12*, 2189.

(14) Powder diffraction file card 29-0836. JCPDS: International Center for Diffraction Data, 1601 Park Lane, Swarthmore, PA 19081.

(15) Powder diffraction file card 20-0631. JCPDS: International Center for Diffraction Data, 1601 Park Lane, Swarthmore, PA 19081.

(16) Powder diffraction file card 04-0664. JCPDS: International Center for Diffraction Data, 1601 Park Lane, Swarthmore, PA 19081.

(17) Powder diffraction file card 22-1142. JCPDS: International Center for Diffraction Data, 1601 Park Lane, Swarthmore, PA 19081.

(18) Gitmans, F.; Sitar, Z.; Günter, P. *Vacuum* **1995**, *46*, 939.

(19) Moulder, J. F.; Stickle, W. F.; Sobol, P. E.; Bomben, K. D. *Handbook of X-ray Photoelectron Spectroscopy*; Perkin-Elmer: Minnesota, 1992.

(20) Repelin, Y.; Husson, E.; Bennani, F.; Proust, C. *J. Phys. Chem. Solids* **1999**, *60*, 819.

(21) Bates, R. B.; Kroposki, L. M.; Potter, D. E.; *J. Org. Chem.* **1972**, *37*, 560.

(22) Powder diffraction file card 25-0922. JCPDS: International Center for Diffraction Data, 1601 Park Lane, Swarthmore, PA 19081.

(23) Powder diffraction file card 18-0749. JCPDS: International Center for Diffraction Data, 1601 Park Lane, Swarthmore, PA 19081.

(24) Powder diffraction file card 74-1646. JCPDS: International Center for Diffraction Data, 1601 Park Lane, Swarthmore, PA 19081.

(25) Powder diffraction file card 70-1566. JCPDS: International Center for Diffraction Data, 1601 Park Lane, Swarthmore, PA 19081.

(26) Bradley, D. C.; Thomas, I. M. *Can. J.   Chem.* **1962**, *40*, 449.

(27) Powder diffraction file card 16-0459. JCPDS: International Center for Diffraction Data, 1601 Park Lane, Swarthmore, PA 19081.
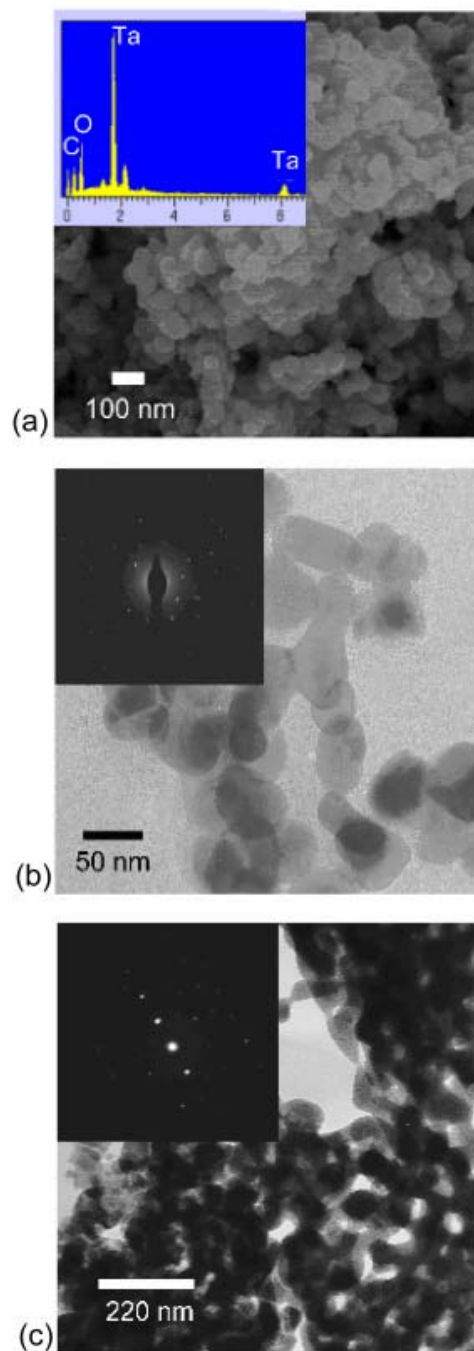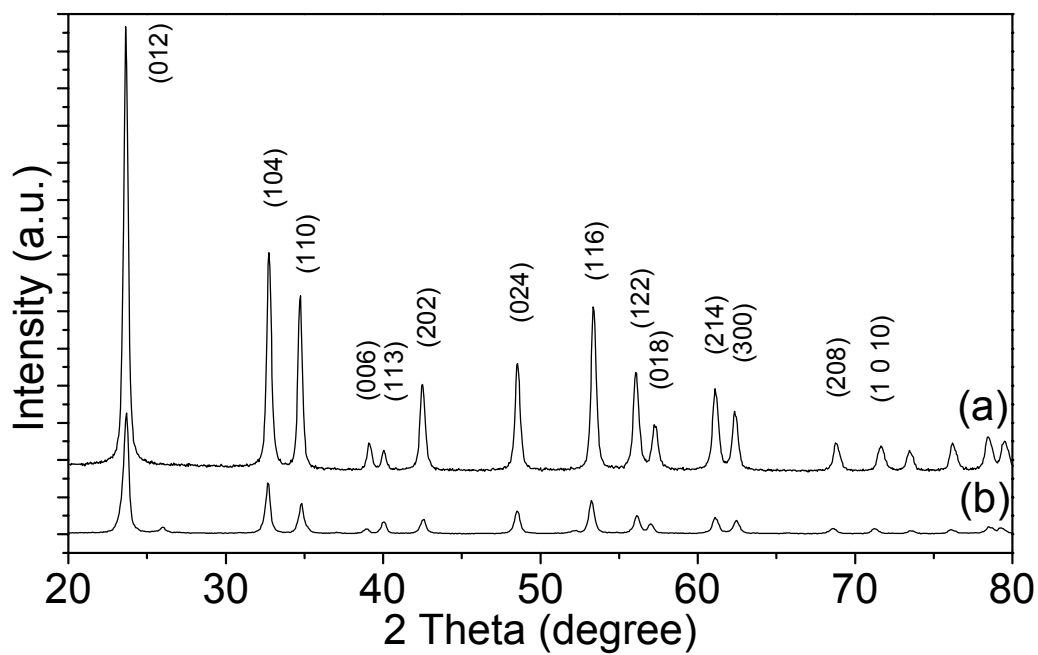
Fig. 2-1 LiTaO$_3$ nanopowders prepared from TaCl$_5$ and alkyllithiums in THF followed by heat treatment. (a) SEM and EDS (inset), from [n]BuLi then processed at 873 K; (b) TEM and ED (inset), from [n]BuLi then processed at 773 K; (c) TEM and ED (inset) from EtLi then processed at 973 K.
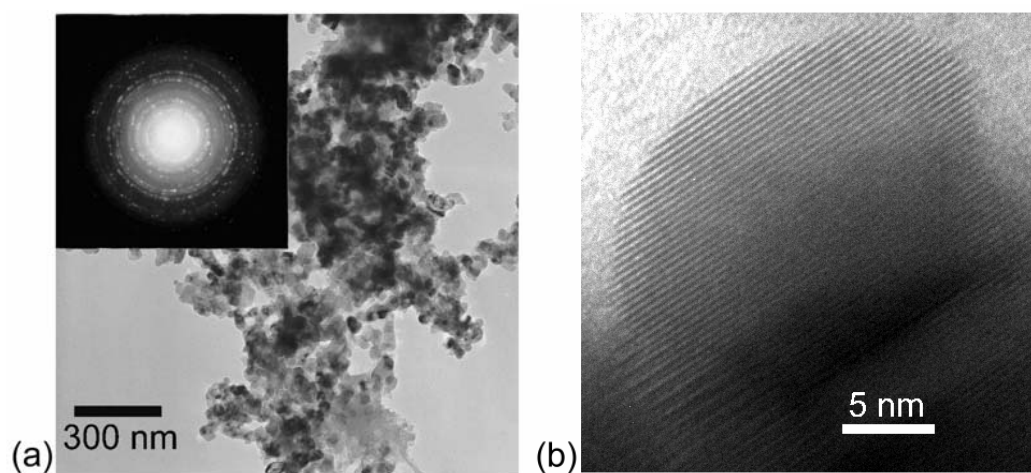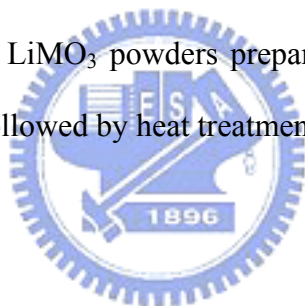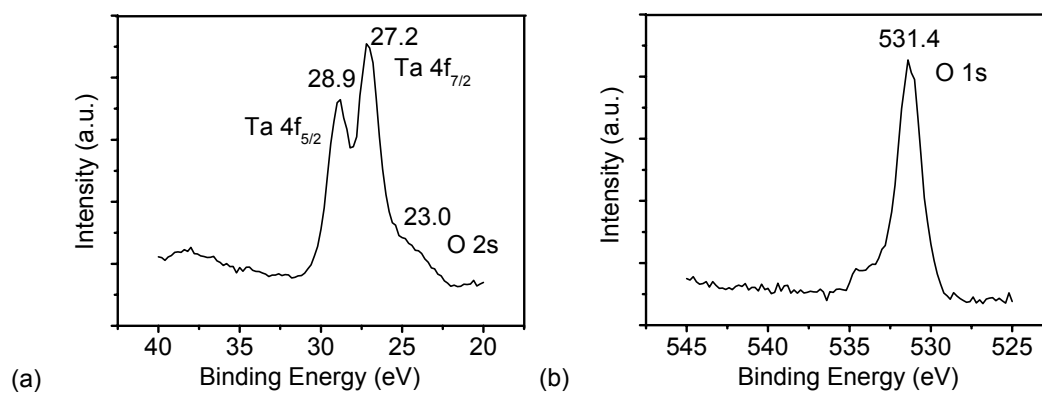
Fig. 2-2 LiNbO$_3$ nanopowders prepared from NbCl$_5$ and EtLi in THF followed by heat treatment at 873 K. (a) TEM and ED (inset). (b) High-resolution TEM image.

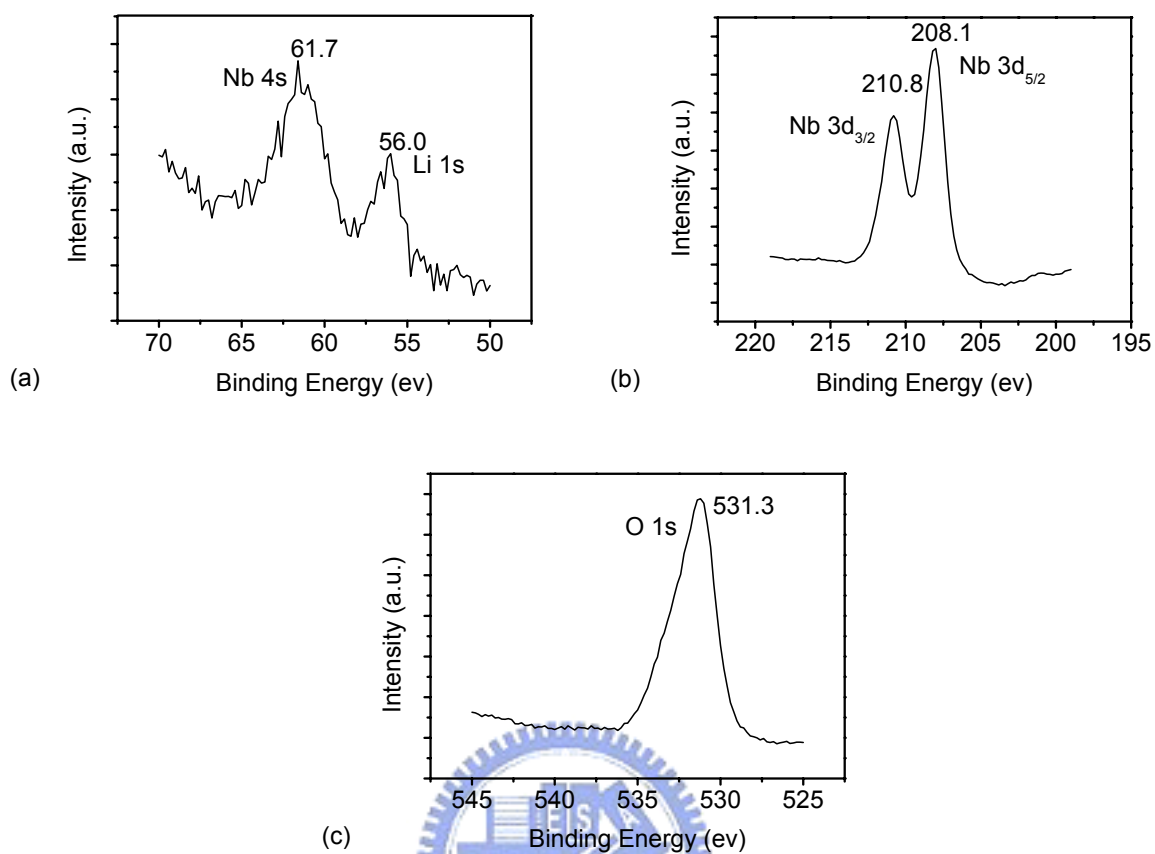**Fig. 2-3** XRD patterns of the $LiMO_3$ powders prepared (a) from $TaCl_5$ and ^nBuLi and (b) from $NbCl_5$ and EtLi in THF followed by heat treatment at 773K under vacuum for 1 h.
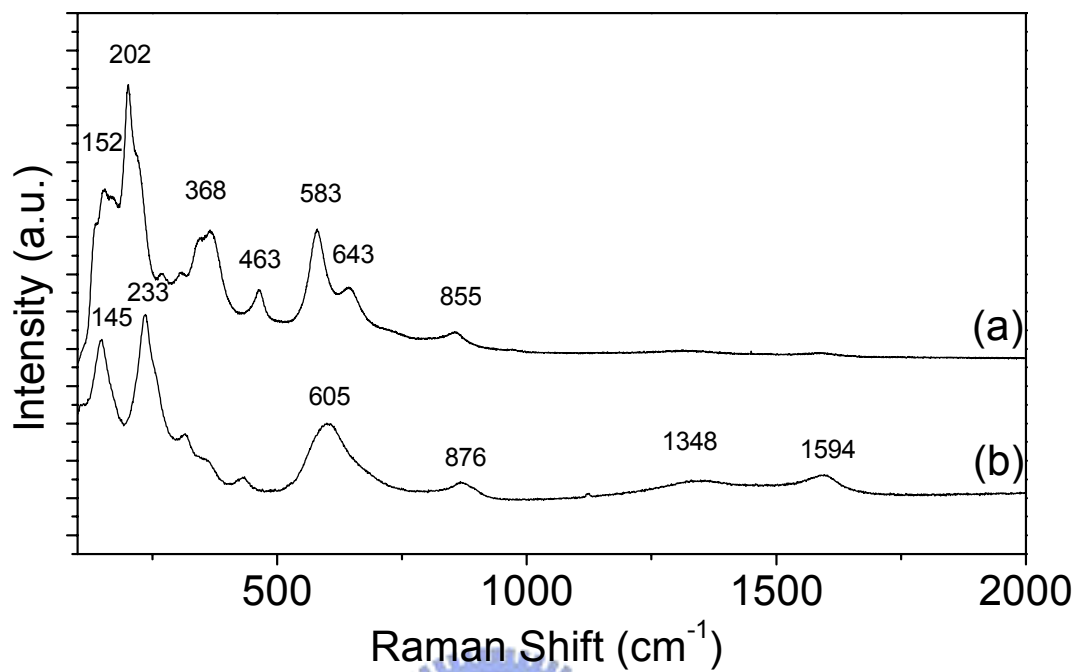
Fig. 2-4 High-resolution XPS of the LiTaO$_3$ prepared from TaCl$_5$ and ^{n}BuLi in THF followed by heat treatment at 973 K. (a) Ta 4f$_{5/2}$, Ta 4f$_{7/2}$, and O 2s electrons, and (b) O 1s electron.
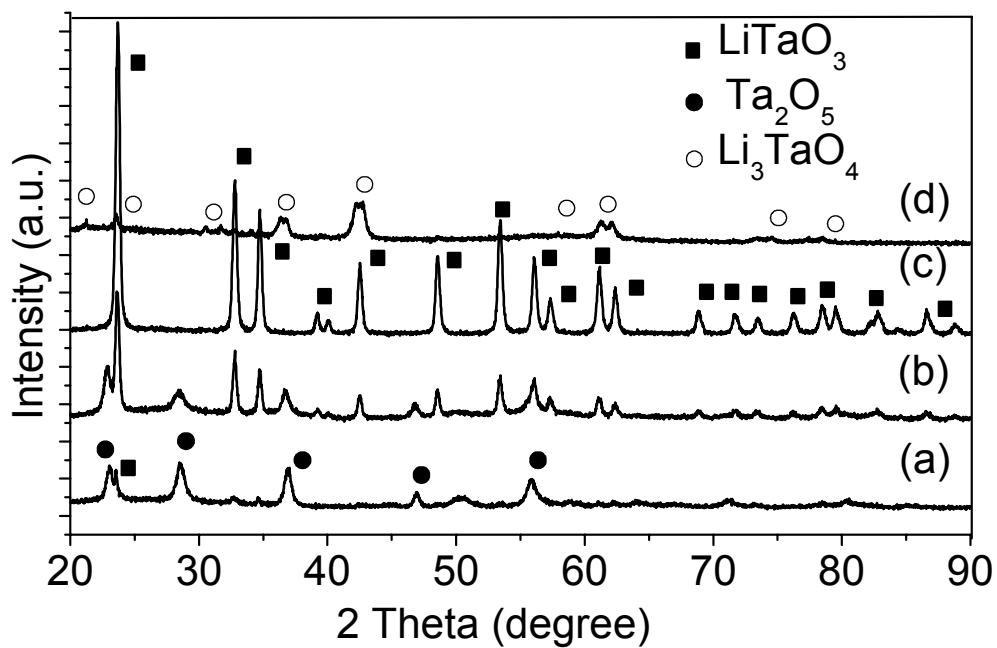
Fig. 2-5 High-resolution XPS signals of (a) Li 1s (together with Nb 4s) (b) Nb $3d_{3/2}$ and Nb $3d_{5/2}$, and (c) O 1s electrons of $LiNbO_3$ nanoparticles prepared at 773 K.
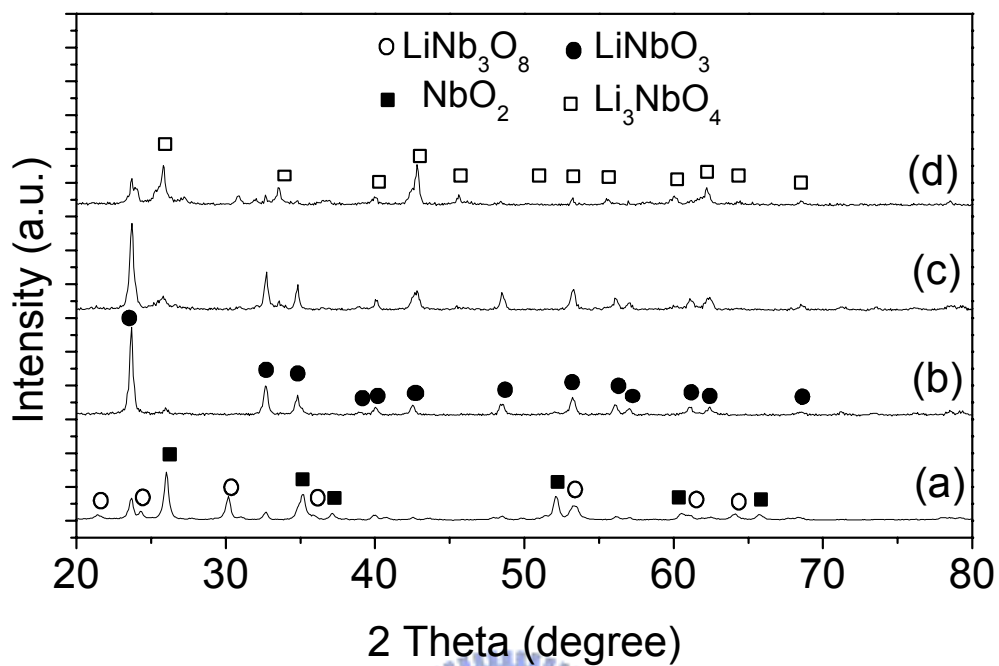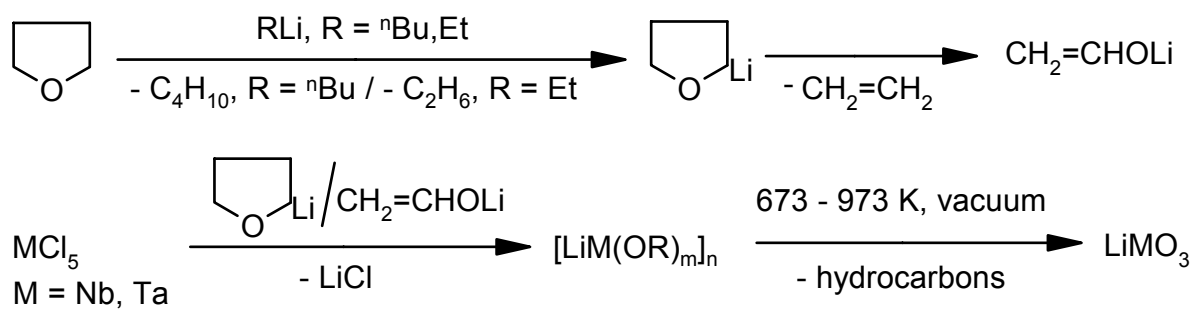
Fig. 2-6 Raman spectra of (a) LiTaO$_3$ and (b) LiNbO$_3$.

Fig. 2-7 XRD patterns of samples prepared from reacting TaCl₅ with EtLi (a) 1 eq, (b) 5 eq, (c) 6 eq, and (d) 8 eq in THF followed by heat-treatment under vacuum at 973 K.

Fig. 2-8 XRD patterns of samples prepared from reacting NbCl$_5$ with EtLi (a) 1 eq, (b) 4 eq,

(c) 5 eq, and (d) 6 eq in THF followed by heat-treatment under vacuum at 873 K.

Reaction scheme:

Tetrahydrofuran $\xrightarrow[\text{- } C_4H_{10}, R = {}^nBu \text{ / - } C_2H_6, R = Et]{\text{RLi, } R = {}^nBu, Et}$ (2-lithio-THF) $\xrightarrow[\text{- } CH_2=CH_2]{}$ $CH_2=CHOLi$

MCl_5
$M = Nb, Ta$ $\xrightarrow[\text{- LiCl}]{\text{(THF-Li) / } CH_2=CHOLi}$ $[LiM(OR)_m]_n$ $\xrightarrow[\text{- hydrocarbons}]{673 - 973 \text{ K, vacuum}}$ $LiMO_3$

Scheme 2-1 Proposed reaction pathway

Chapter 3: Novel route to Synthesize LiMoO$_2$ powders

3.1 Introduction

LiMoO$_2$ offer promising characteristics as a potential cathode-active material for lithium ion application.[1,2] Literature methods used to prepare pure Li$_x$MoO$_2$ phase have relied on (i) reaction of MoO$_2$ with n-butyllithium,[3] (ii) reduction of Li$_2$MoO$_4$ with Mo metal,[4] (iii) lithium insertion in MoO$_2$ using an electrochemical cell,[5] (iv) a two-step synthesis carbothermal reduction (CTR) method,[1,2] and (v) Conversion of MoO(OH) to layered crystalline LiMoO$_2$ upon reaction with Li$_2$CO$_3$ at 873 K in vacuo.[6] In the following we report a different approach to obtain LiMoO$_2$ powders by using a precursor prepared from ethyllithium (EtLi) and MoCl$_5$.

3.2 Experimental procedure

To MoCl$_5$ (2.0 g, 7.3 mmol, Strem) dissolved in THF (50 mL, Aldrich), EtLi (1.32 g, 15 mmol) was added. EtLi was synthesized by reacting EtBr and Li in pentane and sublimed before use. The reaction mixture was stirred under nitrogen for 2 h. Then, it was stirred for 48 h more in air. After the solvent was removed under vacuum, a black solid was separated. Heating the solid at 873 K under vacuum for 1 h offered a gray powder. The powder was washed several times with deionized water and dried in air at 373 K. (0.43g, 44 % yield based on MoCl$_5$). The product was characterized by scanning electron microscopy (SEM, JEOL JSM-6330F at 15 kV), X-ray diffraction (XRD, Bruker D8 Advance, Cu Kα radiation, 40 kV, and 40 mA), and X-ray photoelectron spectroscopy (XPS, Perkin-Elmer PHI-1600, Mg Kα at 1253.6 eV, binding energy (B.E.) reference to In 3d$_{5/2}$ electron at 443.8 eV, Ar$^+$ ions as sputtering source at 5 kV, 25 mA).

3.3 Results and discussion

In general, the reactions between $MoCl_5$ and EtLi, in THF generated dark colloidal solutions. The colloids were further exposed to air before the heat treatment for a more complete oxidation. For the synthesis of $LiMoO_2$, long exposing time was necessary. IR study of the precursor prepared by $MoCl_5$ and 4 eq EtLi in THF indicated the presence of the vibration from CO_3^{2-}. We propose the Li_2CO_3 was formed in the exposing time. The LiOH generated from the reaction between EtLi and the moisture may absorb CO_2 in the air. Li_2CO_3 was excellent Li source in the $LiMoO_2$ synthesis.[1-2,6]

The stoichiometry relation between $MoCl_5$ and ethyllithium (EtLi) is essential for the synthesis of $LiMoO_2$. In a series of precursor preparations, the ratios of $MoCl_5$ to EtLi were varied from 1:1 to 1:6. Then, the products isolated from the precursors heated at 873 K were studied by X-ray diffraction (XRD) in Fig. 3-1. In a Li deficient experiment, when only 1:1 ratio of $MoCl_5$ to EtLi was employed, MoO_2 was the major product, as indicated by the pattern in Fig. 3-1(a). Fig. 3-1(b) shows a mixture of $LiMoO_2$ and MoO_2, the products prepared from 1:4 ratio of $MoCl_5$ and EtLi.[7,8] As the amount of EtLi was increased to 5 eq, isolation of a mixture of $LiMoO_2$, Li_2MoO_4 and a small amount of Mo_2C is shown in Fig. 3-1(c).[7-9] Employing 6 eq of EtLi in the reaction produces more Li_2MoO_4, as shown in Fig. 3-1(d).[8] To remove excess Li_2MoO_4, the powder shown in Fig. 3-1(c) is washed by deionized water to display the pattern of pure $LiMoO_2$ in Fig. 3-1(e). The XRD pattern shows reflections at $2\theta = 17.38, 36.19, 37.69, 43.06$ and 46.78, corresponding to the $LiMoO_2$ (003), (101), (102), (104) and (015) reflections, respectively.[7] The signal at 39.2 degree may indicate that the sample contains small amount of Mo_2C.[9] No other molybdates, such as Li_2MoO_4 and MoO_2, are detected in the sample.

The heat treatment temperature affects the product formation significantly. The XRD patterns of samples prepared from reacting $MoCl_5$ with 5 eq EtLi at 473 – 973 K was shown in Fig. 3-2. When a temperature of 473 – 573 K was employed, the XRD patterns of the products could only be indexed to Li_2MoO_4. Only when a higher temperature of 673 – 973 K

was employed, the mixture of $LiMoO_2$ and Li_2MoO_4 can be observed. A scanning electron micrograph (SEM) of $LiMoO_2$ reveals that the particle size is about 300 nm − 1 μ m [Fig. 3-3].

A survey X-ray photoelectron spectrum (XPS) of the $LiMoO_2$ powder showed the signals of Li, Mo, O and C (weak). In the high-resolution spectrum in Fig. 3-4(a), a very weak signal at 54.5 eV is assigned to the binding energy (b.e.) of Li 1s electron.[10] Two peaks at b.e. of 231.8 and 229.0 eV, as shown in Fig. 3-4(b), are assigned to Mo $3d_{3/2}$ and Mo $3d_{5/2}$ electrons in the middle oxidation state, respectively.[10] A strong peak at 530.5 eV in Fig. 3-4(c) is assigned to the O 1s electron in a metal oxide environment.[10]

3.4 Conclusions

We have successfully synthesized $LiMoO_2$ powders from a precursor prepared by reacting EtLi and $MoCl_5$ in THF followed by a long time oxidation. We speculate that $LiMoO_2$ was synthesized by the reaction between molybdenum oxides and Li_2CO_3 assisted from CO_2 in the air. Detailed studies are in progress.

3.5 References

(1) Barker, J.; Saidi, M. Y.; Swoyer, J. L. *Electrochem. Solid-State Lett.* **2003,** *6*, A252.

(2) Barker, J.; Saidi, M. Y.; Swoyer, J. L. *Solid State Ionics* **2003,** *158*, 261.

(3) Cox, D. E.; Cava, R. J.; McWhan, D. B.; Murphy, D. W. *J. Phys. Chem. Solids* **1982,** *43*, 657.

(4) Aleandri, L. E.; McCarley, R. E. *Inorg. Chem.* **1988,** *27*, 1041.

(5) Huang, C.-K.; Crouch-Baker, S.; Huggins, R. A. *J. Electrochem. Soc.* **1988,** 135, 408.

(6) Hollingshead, J. A.; Tyszkiewicz, M. T.; McCarley, R. E. *Chem. Mater.* **1993,** *5*, 1600.

(7) Powder diffraction file card 47-1127. JCPDS: International Center for Diffraction Data, 1601 Park Lane, Swarthmore, PA 19081.

(8) Powder diffraction file card 12-0763. JCPDS: International Center for Diffraction Data, 1601 Park Lane, Swarthmore, PA 19081.

(9) Powder diffraction file card 11-0680. JCPDS: International Center for Diffraction Data, 1601 Park Lane, Swarthmore, PA 19081.

(10) Moulder, J. F.; Stickle, W. F.; Sobol, P. E.; Bomben, K. D. in: *Handbook of X-ray Photoelectron Spectroscopy*, Perkin-Elmer: Minnesota, 1992.
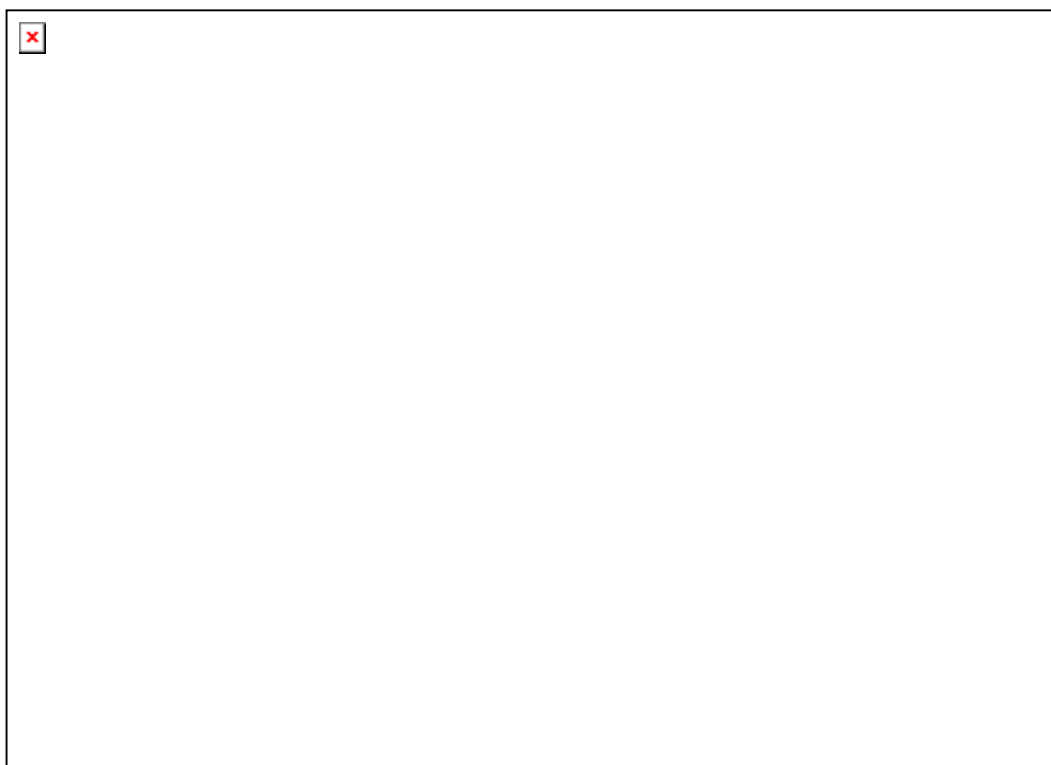
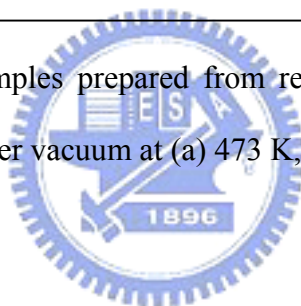**Fig. 3-1** XRD patterns of samples prepared from reacting MoCl$_5$ with EtLi (a) 1 eq, (b) 4 eq, (c) 5 eq, and (d) 6 eq in THF followed by heat-treatment under vacuum at 873 K for 1h. (e) Formed by washing sample (c) with deionized water.
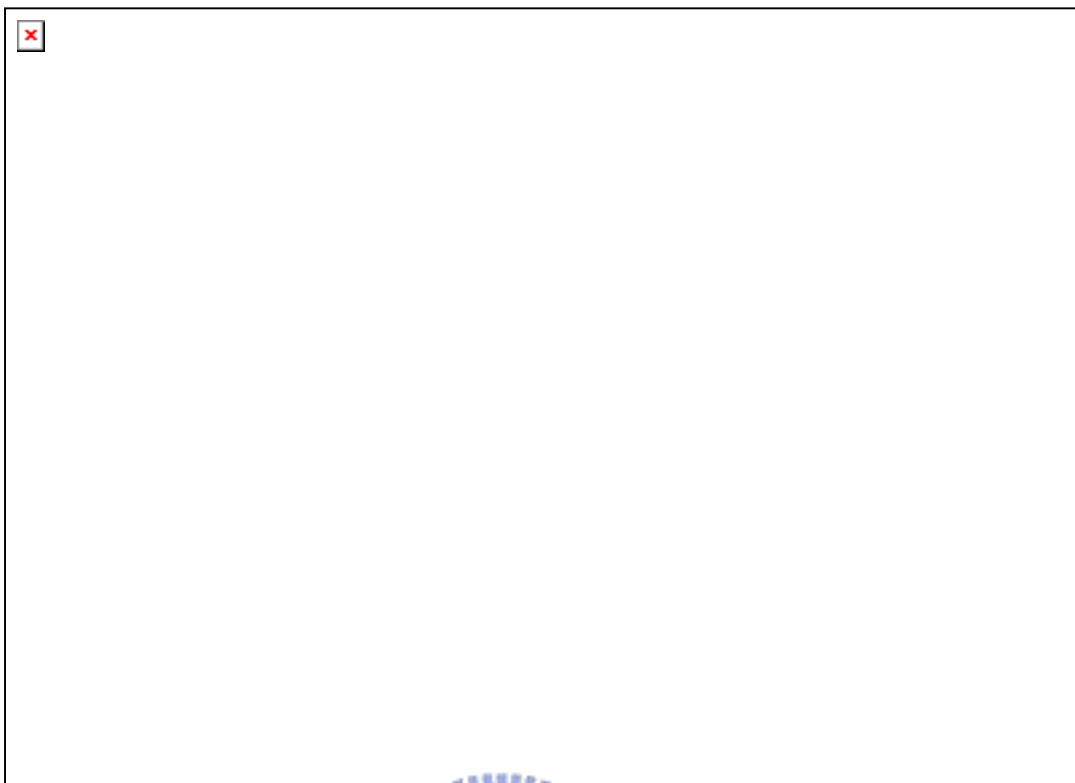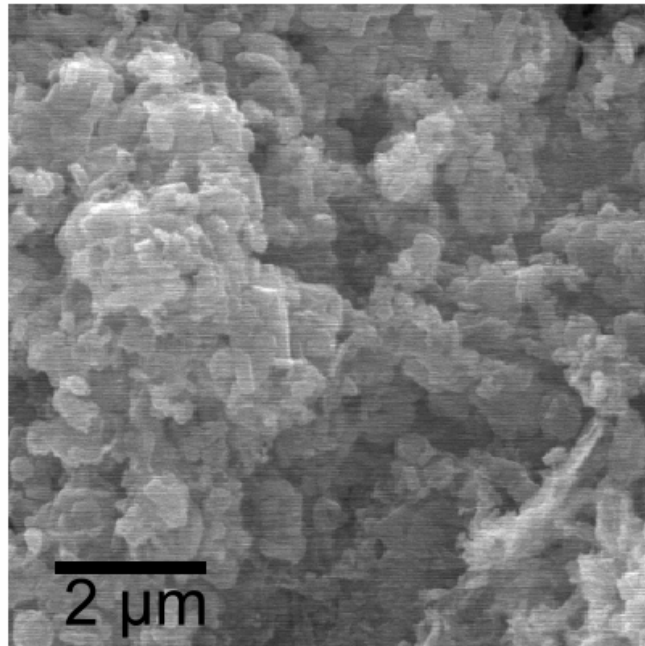
Fig. 3-2 XRD patterns of samples prepared from reacting MoCl₅ with 5 eq EtLi in THF followed by heat-treatment under vacuum at (a) 473 K, (b) 673 K, and (c) 973 K for 1h.

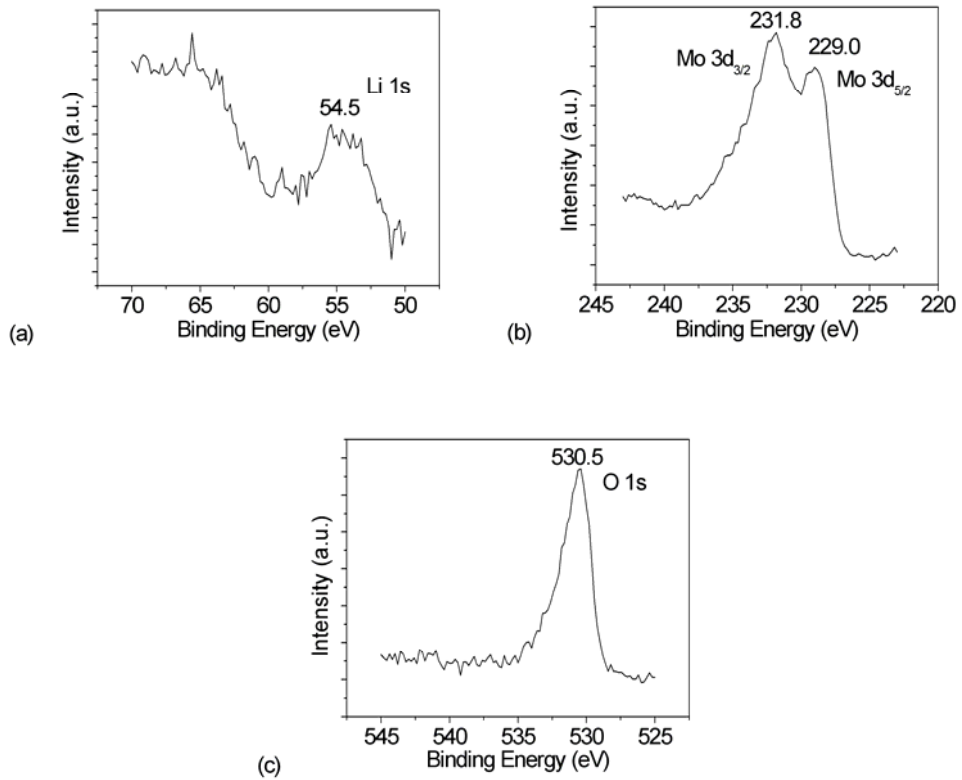**Fig. 3-3** SEM image of LiMoO$_2$ powders.

Fig. 3-4 High-resolution XPS signals of (a) Li 1s (b) Mo $3d_{3/2}$ and Mo $3d_{5/2}$, and (c) O 1s electrons of $LiMoO_2$.

Chapter 4: Synthesis of molybdenum carbides from colloidal precursors prepared in solutions

4.1 Introduction

Molybdenum carbide has been examined as a catalyst for many reactions because the reactivity is often similar to that of platinum group metals.[1-10] Nanostructured molybdenum carbide has been prepared by several solution phase chemical reductions and solid state carbothermal reductions.[11-18] Other potential routes include sonication, reactive-layer assisted deposition and CVD.[19-22] Previously, we reported a method to synthesize nano-sized groups 4 and 5 early transition metal carbides from colloidal precursors generated by reducing metal chlorides with n-butyllithium in hexane.[23] In this report, we widen the reaction methodology and present several new facile syntheses of nanocrystalline Mo_2C particles.
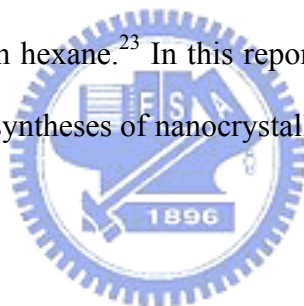
4.2 Experimental Section

4.2.1 General Procedures

Except where it is noted, air and moisture free environment was maintained through the experiment. $MoCl_5$ was purchased from Strem and used without purification. ^nBuLi and THF were supplied by Aldrich. LiH was purchased from Fluka.

4.2.2 Instrumentation

X-ray diffraction (XRD) studies were carried out using a Bruker AXS D8 Advanced diffractometer with Cu Kα radiation. Scanning electron microscopic (SEM) images and energy dispersive spectra (EDS) were collected using a JEOL JSM-6330F at 15 kV. Transmission electron microscopic (TEM) and electron diffraction (ED) images were obtained on a Philips TECNAI 20. Combustion element analyses were performed on a Heraeus CHN-O Rapid instrument.

The synthesis below is used as a general description of the reactions studied in this report. Variation of the reaction conditions and the results are summarized in Scheme 4-1 and Table 4-1.

4.2.3 Synthesis of Mo$_2$C and Mo from colloid precursor formed from MoCl$_5$ and ^{n}BuLi in hexane

To MoCl$_5$ (2.3 g, 8.4 mmol) dissolved in hexane (100 mL), ^{n}BuLi (15 mL, 2.8 M, 42 mmol) was added to form an air-sensitive black precipitate. The reaction mixture was stirred under nitrogen for 4 h. After the solvent was removed in vacuum, a black solid was isolated. Then, the solid was heated at 973 K under vacuum for 1 h to form a grey powder. (0.75 g, 44 % yield of Mo$_2$C and 43 % yield of Mo based on MoCl$_5$. The ratios were estimated from relative XRD intensities.)
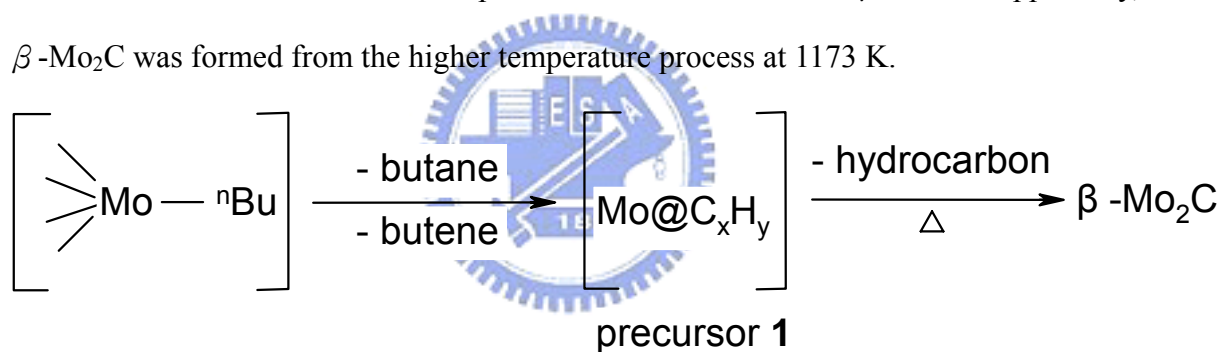
4.3 Results and Discussion

As shown in Scheme 4-1, MoCl$_5$ suspended in hexane or a solution of hexane and THF was allowed to react with ^{n}BuLi or LiH via one of routes (1) – (3). Then, from the reaction, a black colloidal product was isolated and heat-treated at high temperature under vacuum to promote further carbonization and to remove volatile byproducts, including hydrocarbons, CO$_x$ and LiCl. Typical samples obtained from several reaction conditions are summarized in Table 1.

*4.3.1 Synthesis of Mo$_2$C from precursor **1** prepared from MoCl$_5$ and ^{n}BuLi*

Reaction (1) in Scheme 4-1 is a parallel of the previously reported syntheses of group 4 and 5 metal carbides.[18] MoCl$_5$ suspended in hexane was reacted with ^{n}BuLi to generate a dark suspension of colloids. From the suspension, precursor **1** was obtained after the solvent was removed and the precipitate was heated at a high temperature. Fig. 4-1 shows representative SEM images of the isolated powders processed at 773 and 1173 K. Particle size of the powder shown in Fig. 4-1(a) is ca. 200 nm. EDS analysis indicates presence of Mo, C, O and Cl in the

sample. The presence of O suggests possible partial oxidation of the sample during the process. The residual Cl signal points out incomplete replacement of the element in the reaction. SEM and EDS of the sample processed at 1173 K are shown in Fig. 4-1(b). The higher temperature annealing not only increased the size of the powder agglomerates to an average of 5 μm but reduced the O and Cl contamination also. EDS confirms that the sample is composed of Mo and C only while O and Cl levels are significantly decreased. XRD study of the samples is shown in Fig. 4-2. The patterns can be indexed to a mixture of Mo, with a face-centred cubic (fcc) phase and β-Mo$_2$C, with a hexagonal phase.[24,25] Clearly, high temperature treatment increased the signal intensities. This is the result of increase of size and atomic ordering of the particles. From relative ratio of the signal intensities, we conclude that the solids contain comparative amounts of Mo and β-Mo$_2$C. Apparently, more β-Mo$_2$C was formed from the higher temperature process at 1173 K.

$$\left[\begin{array}{c} \diagup \\ \diagdown \end{array} \text{Mo} \!-\! \text{^{n}Bu} \right] \xrightarrow[\text{- butene}]{\text{- butane}} \left[\text{Mo@C}_x\text{H}_y \right] \xrightarrow[\triangle]{\text{- hydrocarbon}} \beta\text{-Mo}_2\text{C}$$

precursor **1**

As shown in the equation above, we propose that reaction (1) in Scheme 4-1 probably proceeds via steps similar to the ones reported previously, a serial combination of metathetic reaction between Mo-Cl and Li-^{n}Bu bonds, β-hydrogen elimination from Mo-^{n}Bu fragments, and reductive elimination of alkanes from Mo-^{n}Bu and Mo-H moieties.[23] The last step probably provides a route to reduce MoCl$_5$ to Mo. Since the combination of MoCl$_5$ and ^{n}BuLi may also form a Ziegler-Natta type catalyst system,[26] we speculate that the alkenes formed in the reaction may further polymerize into a layer of hydrocarbon material which covers the Mo particles to produce Mo@C$_x$H$_y$ in **1**. The direct Mo-C bonding formed from the alkylation and the residual alkyl fragments in **1** also offers a convenient source of carbon. The thermal decomposition of these carbon-rich species probably carbonized Mo to Mo$_2$C.[17]

*4.3.2 Synthesis of Mo₂C from precursor **2** prepared from MoOCl₃(THF)₂ and ⁿBuLi*

In order to prepare more uniformly distributed particle precursors, we converted $MoCl_5$,

which has low solubility in many common solvents, to $MoOCl_3(THF)_2$ first by reacting

$MoCl_5$ with THF.[27] Then, as shown in reaction (2) in Scheme 4-1, $MoOCl_3(THF)_2$ was

allowed to react with ⁿBuLi to form colloidal precursor **2**. Fig. 4-3 shows representative SEM

and TEM images of powders processed from **2** at 1073 and 1173 K. Fig. 4-3(a) displays fine

and uniform particle morphology with an approximate size of 30 nm for the sample produced

at 1073 K. EDS shows presence of Mo and C, and traces of Si and O in the sample. We

speculate that the source of Si was from glass container etched during the process. Fig. 4-3(b)

shows the SEM and EDS of the sample processed from **2** at 1173 K. Apparently, the particle

size was enlarged. However, the TEM image in Fig. 4-3(c) reveals that the powder is

composed of fine particles with a relatively uniform sizes 10 – 20 nm. The ED pattern in

Fig. 4-3(d) is complicated. Careful analysis of the diffraction rings suggests that the sample

may be a mixture of hexagonal and cubic phases materials.[25,28] Fig. 4-4 shows XRD patterns

of the samples prepared from **2** heated at 973 – 1173 K. Fig. 4-4(a) suggests that the

powder annealed at 973 K is amorphous. Fig. 4-4(b) shows that the sample annealed at 1073

K contains mainly hexagonal β-Mo₂C.[25] Below the major signals, a broaden signal centred at

2θ of 37 degree can be seen. In Fig. 4-4(c), the pattern of the sample processed at 1173 K

shows, in addition to the signals of hexagonal β-Mo₂C, four bulges at 37.56, 43.52, 63.08

and 75.83 degrees. They can be indexed to cubic MoO_xC_y.[28] Some extra low intensity signals

are indexed to hexagonal Mo_5Si_3.[29]

The reaction pathway must be a complex process. At first glance, $MoOCl_3(THF)_2$ reacted

with ⁿBuLi to form **2**. However it is reported in literature that ⁿBuLi can also react with THF

to form $CH_2=CHOLi$ within a reasonable period of time.[30] Thus, in the reaction both -ⁿBu and

-OCH=CH₂ fragments can form bonds to Mo via metathetic reactions and affect the product

composition. These are summarized in the equation below. It is shown in Table 4-1 that the
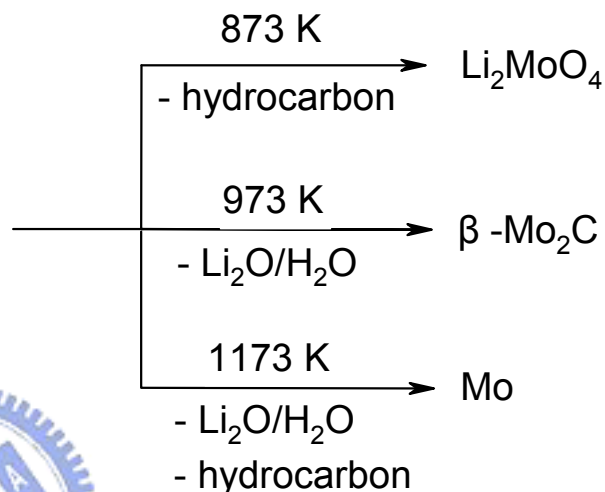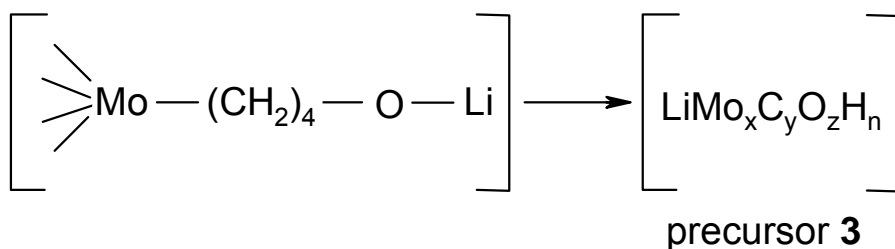
as-prepared carbide contained excess amount of C, probably in the form of amorphous carbon. Also, even though the reaction started with a Mo-oxo complex, $MoOCl_3(THF)_2$, the quantity of O in the samples were insignificant. No pure oxide phase material was detected. Presence of high concentration of C may be resulted from polymerization of unsaturated hydrocarbon fragments formed in the reaction.[26] These carbon rich aggregates $MoC_xO_yH_z$ in **2** may decompose via thermodynamically favoured carbothermal reduction pathways.[17] This is further supported by the following observations

Prolonged exposure of **2** in air formed an O-rich precursor. Fig. 4-5 shows XRD patterns of samples obtained from the precursor heated at high temperatures. XRD pattern of the powder heat treated at 873 K, shown in Fig. 4-5(a), can be indexed to Li_2MoO_4 and MoO_2 crystals.[31,32] In contrast, for the powder prepared at 1073 K, the pattern in Fig. 4-5(b) suggests that Mo was the major component while some hexagonal β-Mo_2C also existed.[24] Heating the precursor at 1273 K generated increased the Mo_2C signals more, as shown in Fig. 4-5(c).[25] The study strongly supports that **2** was carbon rich which facilitates oxygen removal efficiently at high temperatures.[17,33]

The origin of cubic and hexagonal carbides is proposed below. From Mo-^nBu rich or from Mo-OCH=CH$_2$ rich fragments, different composition/structure $MoC_xO_yH_z$ may exist in **2**. They may favour the formation of cubic or hexagonal carbide after thermal decomposition.

In literature, it is shown that MoO_3 can be thermally reduced into different carbide phases by different alkanes.[4,33]

*4.3.3 Synthesis of Mo$_2$C from precursor **3** prepared from MoOCl$_3$(THF)$_2$ and LiH*

In order to search for an alternative reaction process, $MoOCl_3(THF)_2$ was mixed with LiH, instead of ^nBuLi, suspended in a solution of hexane and THF to generate a precursor material, **3** (*Caution:* **3** is explosive above 373 K. Careful control of the temperature ramping is necessary.). Fig. 4-6 shows representative SEM and TEM images of powders prepared from precursor **3** processed at 973 K. Fig. 4-6(a) indicates that particle size of the powder produced at 973 K is about 2 μ m apparently. EDS shows the presence of Mo, C and residual O atoms. TEM and ED images of the sample are shown in Fig. 4-6(b). They reveal that each particle is an aggregate of small particles of ca. 20 nm in size. The lattice parameters estimated from the ED pattern are consistent with the reported values of hexagonal β-Mo$_2$C.[25] Fig. 4-7 shows the XRD patterns of the samples prepared from **3** followed by heat treatment at 873 – 1173 K. Fig. 7(a) shows that the sample processed at 873 K contain two phases which can be indexed to Li_2MoO_4 and hexagonal β-Mo$_2$C.[25,31] For the sample processed at 973 K, only reflections of hexagonal β-Mo$_2$C are present, as shown in Fig. 4-7(b).[25] For the sample heat treated at 1173 K, the XRD pattern in Fig. 4-7(c) shows the presence of Mo only. The carbon source probably originates from the THF molecules since we did not use an organolithium reagent to reduce $MoOCl_3(THF)_2$. The reaction had a temperature threshold at 373 K. Above this temperature, the reaction was initiated and propagated rapidly. In the reaction shown below, we speculate that LiH could remove both coordinated O and Cl ligands from the Mo centre to activate THF and forms an activated precursor material containing Mo-$(CH_2)_4$-OLi linkage. The structure was proposed based on a reported species.[34] High temperature treatment may promote the removal of hydrocarbons to generate Li_2MoO_4, carbonize the metal into carbides or remove all fragments as volatile byproducts to offer the metal.

$$\left[\diagup\!\!\!\!\diagdown Mo-(CH_2)_4-O-Li \right] \longrightarrow \left[LiMo_xC_yO_zH_n \right]$$

precursor **3**

$$\xrightarrow[\text{- hydrocarbon}]{873\ K} Li_2MoO_4$$

$$\xrightarrow[\text{- Li}_2O/H_2O]{973\ K} \beta\text{-Mo}_2C$$

$$\xrightarrow[\substack{\text{- Li}_2O/H_2O \\ \text{- hydrocarbon}}]{1173\ K} Mo$$

4.4 Conclusions

In summary, we have explored several new methods employing colloidal precursors prepared in solutions to synthesize molybdenum carbide particles. Although the reactions appear to be closely related apparently, detailed analysis of the results suggests that the carbonization step in each process varies significantly. In the first reaction, $MoCl_5$ is reduced to **1**, probably composed particles with Mo metal core and carbon shell, by ^nBuLi. Then, at a high temperature, the metal core is by carbonized by the carbon shell to form the carbide. The result is that more Mo and C are converted to β-Mo_2C at higher temperatures. The second investigation is the reduction of $MoOCl_3(THF)_2$ by ^nBuLi in the presence of THF. Because the reactants are hydrocarbon and oxygen-rich, the as-prepared precursor **2** probably contains high C and O contents. We expect that all elements are intermixed in **2** at molecular level. When **2** is decomposed at a high temperature, the excess O atoms probably are removed by the C atoms via carbothermal reduction steps. Formation of two separated carbide phases in

this process is interesting. One of the reasons why they are formed is due to the difference in their thermodynamic stability. However, since in the other two processes only one carbide phase is detected, we speculate that different hydrocarbon fragments in **2** could react via kinetically different pathways to form different carbide phases. And this is more likely to be the reason. In the last reaction investigated, we obtained β-Mo_2C even though the reductant LiH is hydrocarbon free. We propose that in the reaction, when the reactant mixture containing $MoOCl_3(THF)_2$ and LiH are thermally activated, a versatile intermediate material containing elements Mo, C, H, O and Li is produced. At different high temperatures, this material decomposes into several different Mo containing products, including Li_2MoO_4, β-Mo_2C, and Mo. This is another example of the rich chemistry and wide range of oxidation states of Mo compounds. Searching for possible catalytic applications of the carbides prepared in this study is in progress.

4.5 References

(1) Hyeon, T.; Fang, M.; Suslick, K. S. *J. Am. Chem. Soc.* **1996**, *118*, 5492.

(2) Oxley, J. D.; Mdleleni, M. M.; Suslick, K. S. *Catal. Today* **2004**, *88*, 139.

(3) Cuong, P.-H.; Ledoux, M. J.; Guille, J. *J. Catal.* **1993**, *143*, 249.

(4) Xiao, T.-C.; York, A. P. E. ; William, V. C.; Al-Megren, H.; Hanif, A.; Zhou, X.-Y.; Green, M. L. H. *Chem. Mater.* **2000,** *12*, 3896.

(5) Manoli, J.-M.; Costa, P. Da; Brun, M.; Vrinat, M.; Maugé, F.; Potvin, C. *J. Catal.* **2004**, *221*, 365.

(6) Szymańska, A.; Lewandowski, M.; Sayag, C.; Djéga-Mariadassou, G. *J. Catal.* **2003**, *218*, 24.

(7) Pham-Huu, C.; Gallo, P. D.; Peschiera, E.; Ledoux, M. J. *Appl. Catal. A* **1995**, *132*, 77.

(8) Claridge, J. B.; York, A. P. E.; Brungs, A. J.; Marquez-Alvarez, C.; Sloan, J.; Tsang, S. C.; green, M. L. H. *J. Catal.* **1998**, *180*, 85.

(9) Griboval-Constant, A.; Giraudon, J.-M.; Leclercq, G.; Leclercq, L. *Appl. Catal. A* **2004**, *260*, 35.

(10) Oshikawa, K.; Nagai, M.; Omi, S. *J. Phys. Chem. B* **2001**, *105*, 9124.

(11) Zeng, D.; Hampden-Smith, M. J. *Chem. Mater.* **1992**, *4*, 968.

(12) Zeng, D.; Hampden-Smith, M. J. *Chem. Mater.* **1993**, *5*, 681.

(13) Nelson, J. A.; Wagner, M. J. *Chem. Mater.* **2002**, *14*, 1639.

(14) Gu, Y.; Li, Z.; Chen, L.; Ying, Y.; Qian, Y. *Mater. Res. Bull.* **2003**, *38*, 1119.

(15) Preiss, H.; Meyer, C.; Olschewski, C. *J. Mater. Sci.* **1998**, *33*, 712.

(16) Liang, C.; Ying, P.; Li, C.; *Chem. Mater.* **2002,** *14*, 3148.

(17) Chaudhury, S.; Mukerjee, S.K.; Vaidya, V.N.; Venugopal, V. *J. Alloys Compd.* **1997**, *261*, 105.

(18) Nartowski, A. M.; Parkin, I. P.; Mackenzie, M.; Craven, A. J. *J. Mater. Chem.* **2001**, *11*, 3116.

(19) Dantsin, G.; Suslick, K. S. *J. Am. Chem. Soc.* **2000**, *122*, 5214.

(20) Horn, J. M.; Song, Z.; Potapenko, D. V.; Hrbek, J.; White, M. G. *J. Phys. Lett. B* **2005**, *109*, 44.

(21) Chen, H.Y.; Chen, L.; Lu, Y.; Hong, Q.; Chua, H.C.; Tang, S.B.; Lin, J. *Catal. Today* **2004**, *96*, 161.

(22) Lu, J.; Hugosson, H.; Eriksson, O.; Nordström, L.; Jansson, U. *Thin Solid Films* **2000,** *370*, 203.

(23) Chang, Y.-H.; Chiu, C.-W.; Chen, Y.-C.; Wu, C.-C.; Tsai, C.-P.; Wang, J.-L.; Chiu, H.-T. *J. Mater. Chem.* **2002,** *12*, 2189.

(24) Powder diffraction file card 42-1120. JCPDS: International Center for Diffraction Data, 1601 Park Lane, Swarthmore, PA 19081.

(25) Powder diffraction file card 11-0680. JCPDS: International Center for Diffraction Data, 1601 Park Lane, Swarthmore, PA 19081.

(26) Crabtree, R. H. in *The Organometallic Chemistry of the Transition Metals*, A Wiley-Interscience Publication, New York, **2001**.

(27) Feenan, K.; Fowles, G. W. A. *Inorg. Chem.* **1965,** *4*, 310.

(28) Powder diffraction file card 17-0104. JCPDS: International Center for Diffraction Data, 1601 Park Lane, Swarthmore, PA 19081.

(29) Powder diffraction file card 08-0429. JCPDS: International Center for Diffraction Data, 1601 Park Lane, Swarthmore, PA 19081.

(30) Bates, R. B.; Kroposki, L. M.; Potter, D. E. *J. Org. Chem.* **1972,** *37*, 560.

(31) Powder diffraction file card 12-0763. JCPDS: International Center for Diffraction Data, 1601 Park Lane, Swarthmore, PA 19081.

(32) Powder diffraction file card 86-0135. JCPDS: International Center for Diffraction Data, 1601 Park Lane, Swarthmore, PA 19081.

(33) Xiao, T.-C.; York, A. P. E.; Coleman, K. S.; Claridge, J. B.; Sloan, J.; Charnock, J.; Green,
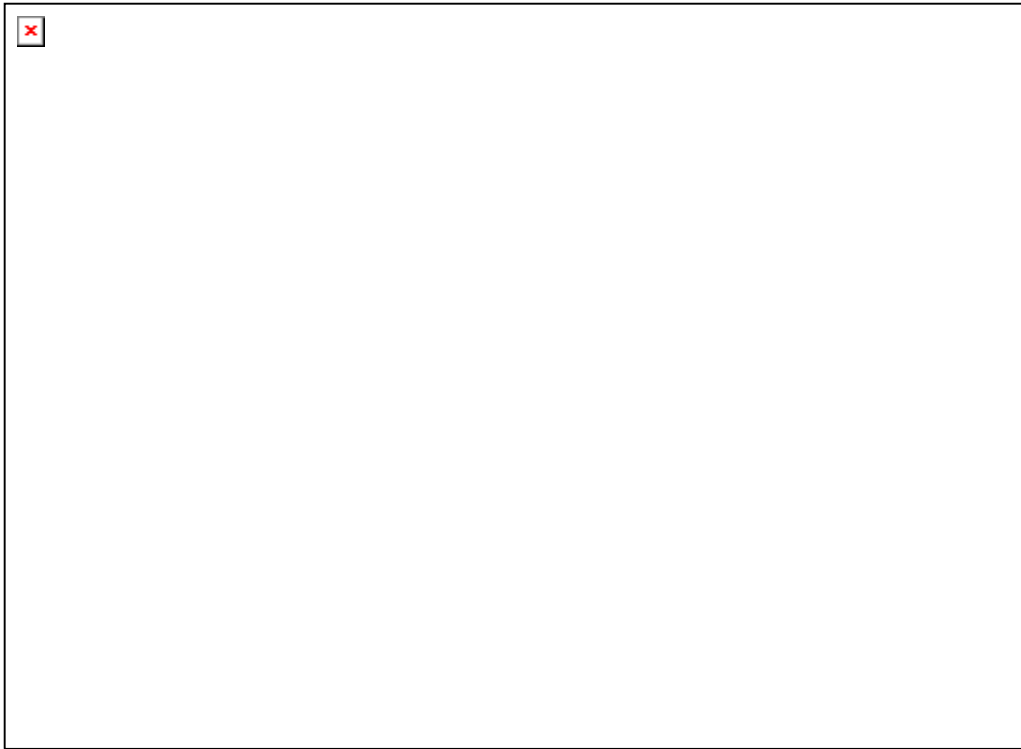
M. L. H. *J. Mater. Chem.* **2001,** *11*, 3094.

(34) Collman, J. P.; Hegedus, L. S.; Norton, J. R.; Finke, R. G. in: *Principles and Application of Organotransition Metal Chemistry*, University Science: BooksBerkeley, CA, **1987**.
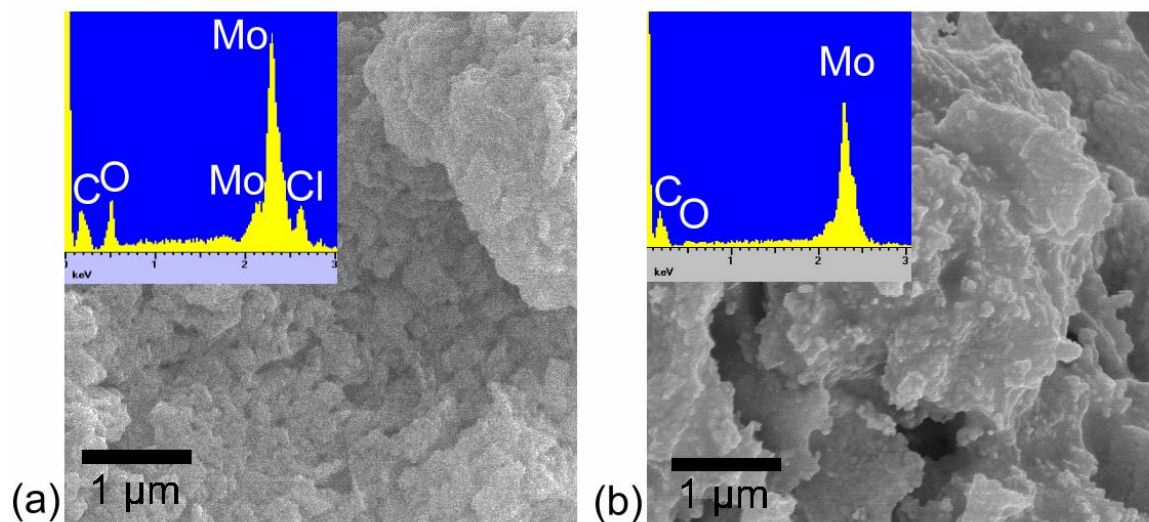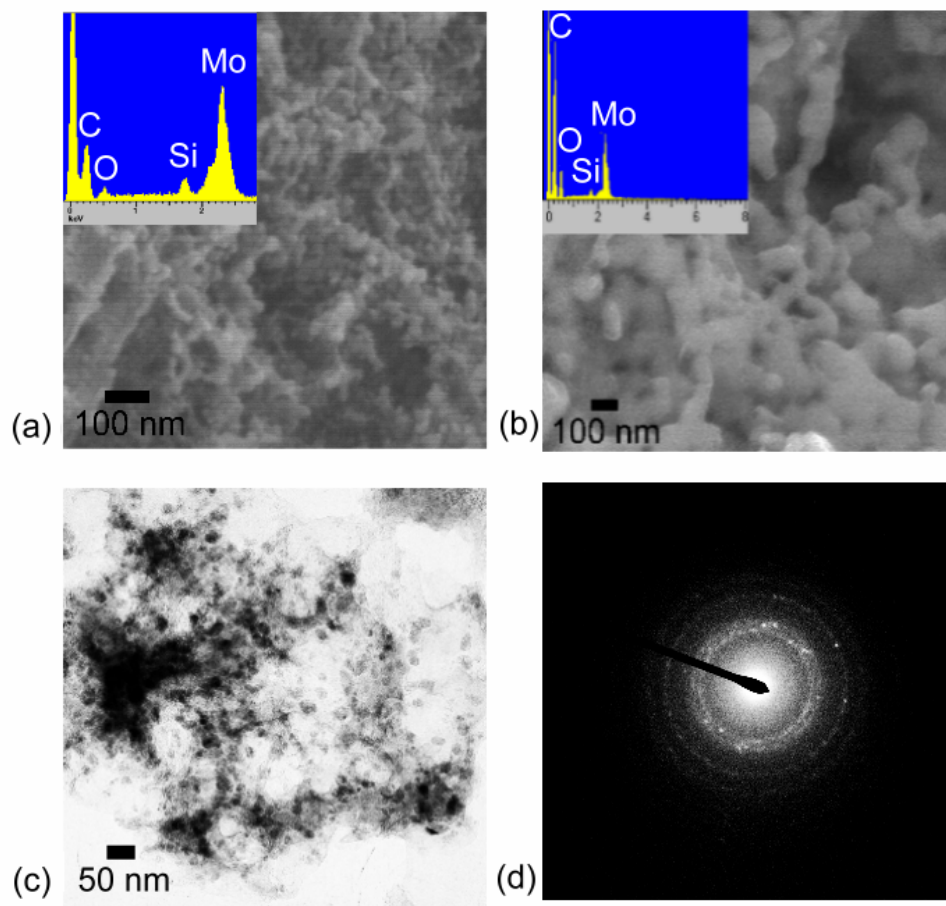
Fig. 4-1 SEM and EDS (inset) images of powders prepared from **1** heat treated at (a) 773 K and (b) 1173 K.
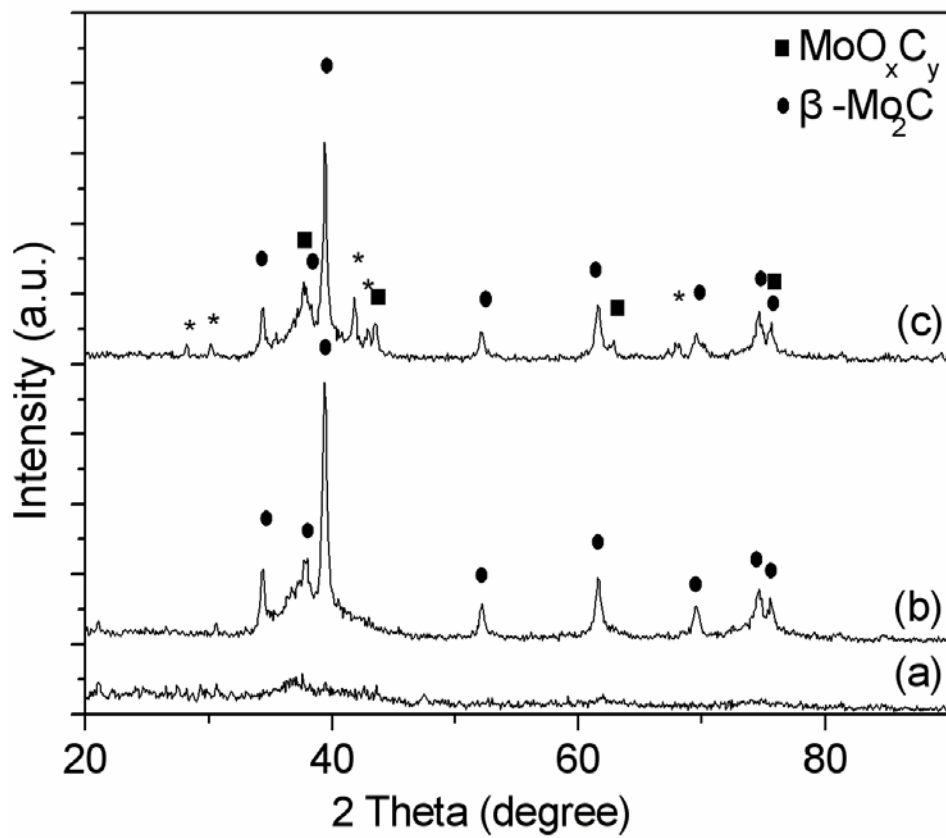
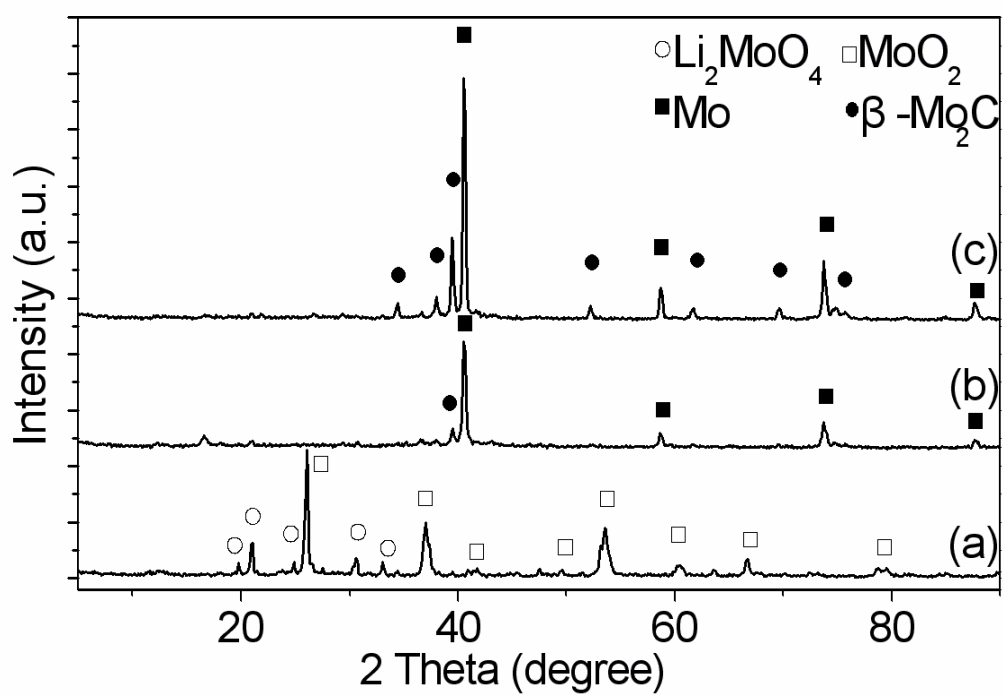**Fig. 4-2** XRD patterns of powders prepared from **1** heat treated at (a) 773 K, (b) 973 K and (c) 1173 K.

Fig. 4-3 SEM and EDS (inset) images of powders prepared from **2** heat treated at (a) 1073 K and (b) 1173 K. (c) TEM image of particles in (b). (d) ED image of particles in (b).
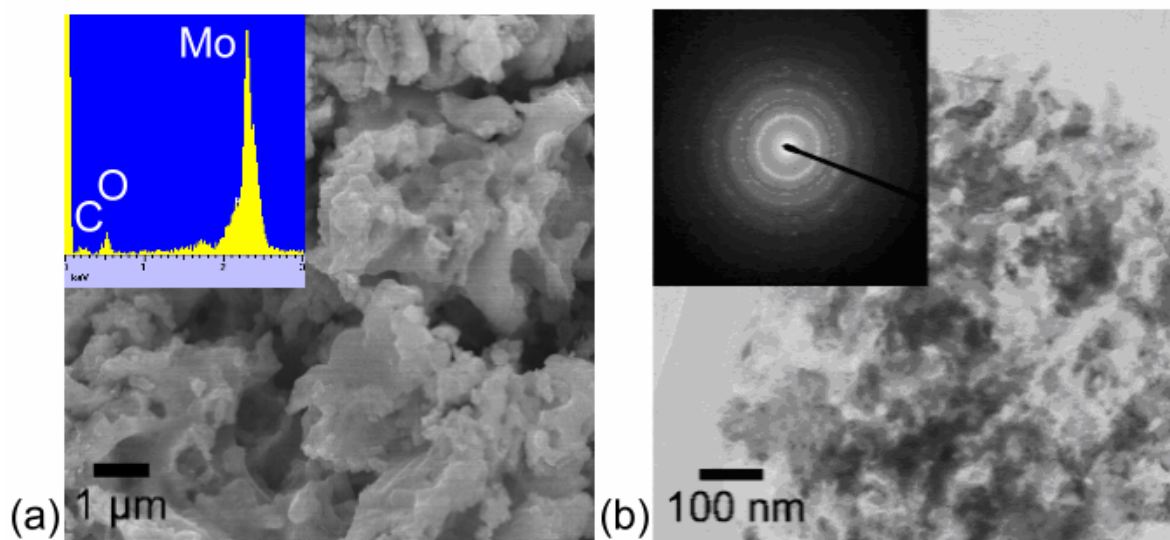
Fig. 4-4 XRD patterns of powders prepared from **2** heat treated at (a) 973 K, (b) 1073 K and
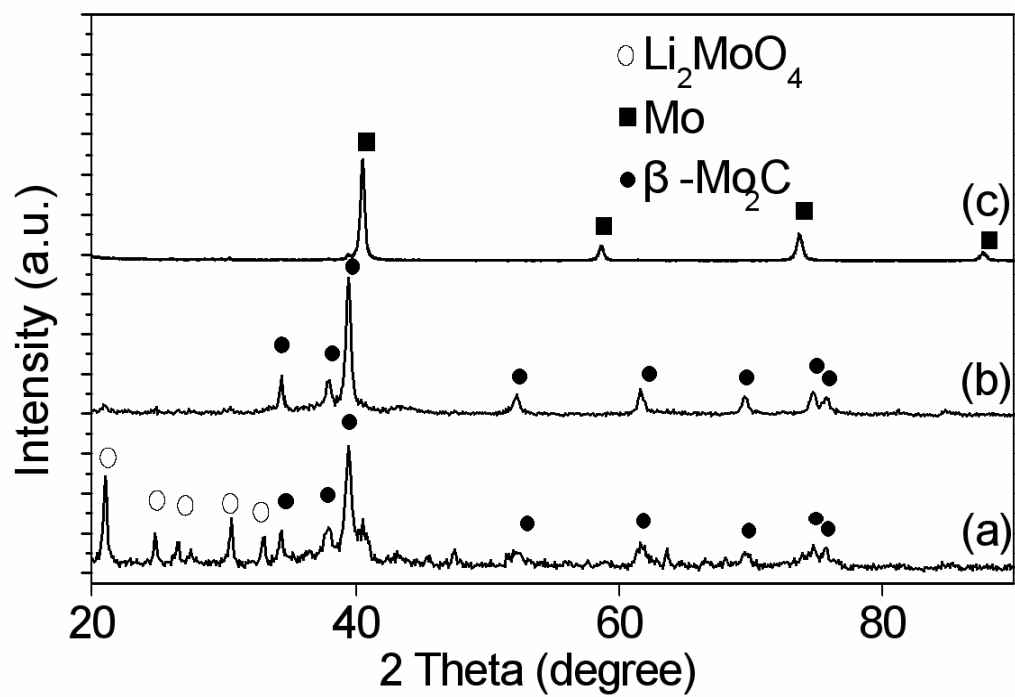
(c) 1173 K. (* Mo_5Si_3)

Fig. 4-5 XRD patterns of powders prepared from **2** stirred in air and heat treated at (a) 873 K,
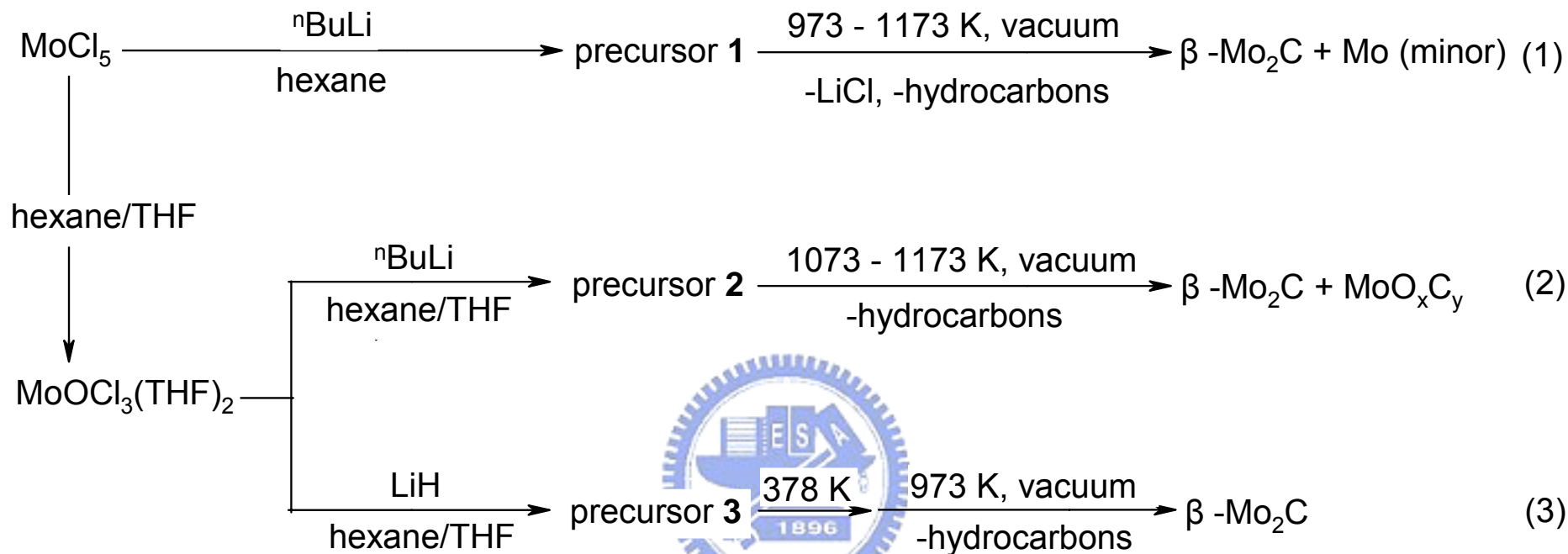
(b) 1073 K and (c) 1273 K.

Fig. 4-6 (a) SEM and EDS (inset) images of Mo_2C powders prepared from **3** heat treated at 973 K. (b) TEM and ED (inset) in (a).

Fig. 4-7 XRD patterns of powders prepared from **3** heat treated at (a) 873 K, (b) 973 K and (c) 1173 K.

$$\text{MoCl}_5 \xrightarrow[\text{hexane}]{^n\text{BuLi}} \textbf{precursor 1} \xrightarrow[\text{-LiCl, -hydrocarbons}]{973 - 1173 \text{ K, vacuum}} \beta\text{-Mo}_2\text{C} + \text{Mo (minor)} \quad (1)$$

MoCl$_5$ → (hexane/THF) → MoOCl$_3$(THF)$_2$

$$\text{MoOCl}_3(\text{THF})_2 \xrightarrow[\text{hexane/THF}]{^n\text{BuLi}} \textbf{precursor 2} \xrightarrow[\text{-hydrocarbons}]{1073 - 1173 \text{ K, vacuum}} \beta\text{-Mo}_2\text{C} + \text{MoO}_x\text{C}_y \quad (2)$$

$$\text{MoOCl}_3(\text{THF})_2 \xrightarrow[\text{hexane/THF}]{\text{LiH}} \textbf{precursor 3} \xrightarrow{378 \text{ K}} \xrightarrow[\text{-hydrocarbons}]{973 \text{ K, vacuum}} \beta\text{-Mo}_2\text{C} \quad (3)$$

Scheme 4-1 Summary of reaction steps to Mo and Mo$_2$C

Table 4-1 Summary of Reaction Results

Sample	Reactants		Solvents (mL)	Atmosphere, Stirring Time (h)	Annealing T (K)	%Yield of β-Mo$_2$C (based on MoCl$_5$/ MoOCl$_3$(THF)$_2$)	Size Range	Elemental Analysis (wt%, C, H, N)
1	MoCl$_5$	^{n}BuLi	hexane, 100	N$_2$, 4	973	44	200 nm-5 μm	2.47, 1.39, 0.36
2	MoOCl$_3$(THF)$_2$	^{n}BuLi	hexane/THF, 100/8	N$_2$, 4	1073	67	10-30 nm	11.52, 1.56, 0.33
3	MoOCl$_3$(THF)$_2$	LiH	hexane/THF, 100/50	N$_2$, 2	973	45	10-30 nm	1.68, 1.28, 0.42

Chapter 5: Preparation of Mo₂C@*a*-C core-shell powders via carburization of Mo particles by 1-chlorobutane and hexachlorobenzene

5.1 Introduction

Molybdenum carbides are conventionally synthesized by a variety of methods, including, arc melting of Mo or its oxide with graphite, temperature-programmed reaction between molybdenum oxide and alkanes, and annealing mechanically activated mixture of amorphous carbon with molybdenum.[1-6] Recent reports have shown that it is possible to prepare Mo_2C through reduction-carburization. For example, high temperature reduction of $MoCl_5$ by a mixture of 20% of CH_4 in H_2 produced Mo_2C.[7] Reduction of MoO_3 powders by carbon black at high temperatures generated Mo_2C also.[8] Similar reaction methodology was employed to prepare activated carbon supported bimetallic carbide of molybdenum and tungsten.[9] Previously, we reported a method to synthesize titanium carbide via carburization of titanium powders by 1-chlorobutane.[10] In another study, we discovered that hexachloroethane could be used to carburize titanium and molybdenum surfaces.[11] In this report, we wish to discuss the result of carburization reaction of molybdenum powders by 1-chlorobutane and hexachlorobenzene. Particularly, we found that Mo₂C@*a*-C particles, with a structure of a Mo_2C core encapsulated in an amorphous carbon shell, can be produced under controlled reaction conditions.

5.2 Experimental Procedure

In a typical reaction, Mo powders (1–3 μm, Riedel-deHaën) in a quartz boat were placed in a 30-mm quartz tube and heated by a horizontal tube furnace at 873–1173 K. At 1

atm, 1-chlorobutane (Janssen) at 298 K was bubbled into the reactor under a flow of Ar (20

sccm) for 8 h to produce a black powder. In another typical reaction, hexachlorobenzene

(Aldrich) at 393 K under vacuum was vaporized and reacted with Mo powders at 1073 K for

24 h to generate a black powder. In all reactions, yellow and brown byproduct solids

deposited at the outlet of the reactor wall. The solids turned green and blue when exposed to

air. The black products were characterized by scanning electron microscopy (SEM, JEOL

JSM-6330F at 15 kV), X-ray diffraction (XRD, Bruker D8 Advance, Cu Kα radiation, 40 kV,

and 40 mA), Raman spectroscopy (Jabin Yvon HR800 equipped with an Ar^{+} laser at 514.5

nm), and X-ray photoelectron spectroscopy (XPS, Perkin-Elmer PHI-1600, MgKα radiation

at 1253.6 eV) Combustion elemental analyses were performed on a Heraeus CHN-O Rapid

instrument to determine the carbon contents.

5.3 Results and discussion

XRD patterns of the solids produced by carburization of Mo powders by 1-chlorobutane

and hexachlorobenzene at 873 – 1173 K for 8 h are shown in Fig. 5-1. Fig. 5-1(a) suggests

that at 873 K, only a small portion of the purchased Mo metal powders was carburized by

1-chlorobutane to form hexagonal Mo_2C.[12,13] At a temperature of 1073 K, the enhanced

signals of Mo_2C, as shown in Fig. 5-1(b), suggest that the reaction proceeded at an increased

rate. Fig. 5-1(c) shows the XRD pattern of the powder prepared at 1173 K. This suggests that

the Mo powders were completely carburized at this temperature. Fig. 5-1(d) shows the XRD

pattern of the sample obtained from the reaction between hexachlorobenzene and Mo at 1073

K. The result also indicates that some Mo was converted into hexagonal Mo_2C.[12,13] The

reaction at 1173 K showed a complete carburization of Mo into Mo_2C in 8 h.

Fig. 5-2(a) shows an SEM image of aggregated particles prepared from 1-chlorobutane

and Mo at 1073 K. EDS is used to study a particular particle marked by arrows **1** and **2**. The

area pointed by **1** is C-rich while the area indicated by **2** is composed mainly of Mo. In both

areas, the signal from Cl is not observed. Fig. 5-2(b) is an enlarged view of the particle. Based on the image, the EDS data, and the XRD in Fig. 5-1(b), we propose that the particle has an inner Mo core with a diameter ca. 2 μm and an outer shell with a thickness ca. 0.5 μm. The shell is composed of Mo_2C and amorphous carbon (see below for amorphous carbon characterization). Fig. 5-2(c) shows an SEM image of the powders prepared from a reaction between hexachlorobenzene and Mo at 1073 K under vacuum. While the original profile of Mo particles is preserved, many holes appear on the surface. We speculate that chlorine atoms etched the Mo surface to form the structure. The process also created particles with reduced sizes. Fig. 5-2(d) reveals that these particles, with size 50 – 200 nm, aggregate together on the surface of Mo. The EDS indicates that the material is still Mo-rich. This is consistent with the XRD data in Fig. 5-1(d), showing the patterns of Mo_2C and Mo.

Fig. 5-3(a) shows a TEM image of aggregated particles prepared from 1-chlorobutane and Mo at 1173 K. The image suggests that the aggregate is covered by a shell with a thickness of ca. 200 nm. An electron diffraction (ED) pattern in Fig. 5-3(b) displays two weak diffused rings. They are indexed to (101) and (110) reflections of small graphite crystals.[14] Due to the sample thickness, the ED pattern of Mo_2C is not observed. Based on the images and XRD result in Fig. 5-1(c), we propose that the sample has a Mo_2C core covered by a less-ordered carbon shell. Even though some small graphite exists in the sample shell, the overall carbon orderness is low. The nearly amorphous nature of the carbon shell is further confirmed by the Raman study below.

Fig. 5-4 shows Raman spectra of the Mo powders carburized by 1-chlorobutane and hexachlorobenzene at different temperatures. The G-band (1589 cm^{-1}) and D-band (1353 cm^{-1}) vibrations suggest the formation of a carbon material. The peak intensity ratio, I_D/I_G, strongly suggests that the observed carbon material in each sample is non-crystalline.[15] The I_D/I_G ratios increase as the reaction temperature was raised from 873 K to 1173 K, as shown in Figs. 5-4(a) - 5-4(c). This suggests that orderness of the carbon atoms decreased slightly at raised reaction

temperatures. Fig. 5-4(d) reveals that the sample, which was prepared by reacting hexachlorobenzene with Mo, also contains amorphous carbon. Fig. 5-5 shows the XPS survey data of a powder prepared from Mo and 1-chlorobutane at 1173 K under a flow of 20 sccm Ar for 8 h. In Fig. 5-5(a), the as-prepared sample shows the presence of Mo and C atoms. No Cl atoms can be detected on the surface. After the sample was sputtered by Ar^+ ion for 30 s, the survey shown in Fig. 5-5(b) indicates that except the intensity of C diminishes slightly, the elemental composition is essentially the same. The carbon content of the sample prepared from Mo and 1-chlorobutane at 1173 K was further investigated by combustion elemental analysis. The result showed that the sample contained 11.68 weight % of C. The theoretical carbon value in Mo_2C is only 5.89 weight %. This suggests that the sample is carbon-rich. Based on this information and the other data shown in Figs. 5-1 - 5-5, we conclude that the material produced at 1173 K in this study is $Mo_2C@a$-C, a completely carburized Mo_2C core wrapped in an amorphous C shell.

A mechanistic model is proposed in Fig. 5-6 to show how a Mo particle is carburized by 1-chlorobutane to form Mo_2C. In the first step, 1-chlorobutane reacts with the Mo surface to deposit an a-C layer. The chlorine atoms combine with Mo atoms to generate volatile $MoCl_x$ molecules, observed as solid deposits at the outlet of the reaction chamber.[16] In the next step, a reaction between a-C and Mo creates an interlayer of Mo_2C between the a-C shell and the Mo core. Finally, further carbon diffusion through the Mo_2C layer causes the inner Mo core to carburize completely into the $Mo_2C@a$-C structure. The reaction process between C_6Cl_6 and Mo powders probably proceeds similarly.

5.4 Conclusions

$Mo_2C@a$-C powders have been synthesized from the reactions between Mo metal powders with 1-chlorobutane or with hexachlorobenzene at 1173 K. The chlorinated reactants not only act as the carbon source to carburize Mo powders but also covered the surface to

form the core/shell structure. The other role of the chlorinated reactants is a source of chlorine atoms, which etched the metal into smaller particles.

5.5 **References**

(1) Hare, J.P.; Hsu, W.K.; Kroto, H.K.; Lappas, A.; Prassides, K.; Terrones, M.; Walton, D.R.M. *Chem. Mater.* **1996,** *8*, 6.

(2) Saito, Y.; Matsumoto, Y.; Nishikubo, K. *J. Crystal Growth* **1997,** *172*, 163.

(3) Xiao, T.-C.; York, A.P.E.; William, V.C.; Al-Megren, H.; Hanif, A.; Zhou, X.-Y.; Green, M.L.H. *Chem. Mater.* **2000,** *12*, 3896.

(4) Xiao, T.; York, A.P.E.; Coleman, K.S.; Claridge, J.B.; Sloan, J.; Charnock, J.; Green, M.L.H. *J. Mater. Chem.* **2001,** *11*, 3094.

(5) Jung, K.T.; Kim, W.B.; Rhee, C.H.; Lee, J.S. *Chem. Mater.* **2004,** *16*, 307.

(6) Bokhonov, B.; Borisova, Y.; Korchagin, M. *Carbon* **2004,** *42*, 2067.

(7) Monteverdi, S.; Mercy, M.; Molina, S.; Bettahar, M.M.; Puricelli, S.; Bégin, D.; Maréche, F.; Furdin, F. *Appl. Catal.* **2002,** *230*, 99.

(8) Chaudhury, S.; Mukerjee, S.K.; Vaidya, V.N.; Venugopal, V. *J. Alloys Compd.* **1997,** *261*, 105.

(9) Nguyen, T.H.; Nguyen, T.V.; Lee, Y.J.; Safinski, T.; Adesina, A.A. *Mater. Res. Bull.* **2005,** *40*, 149.

(10) Lee, C.-Y. *J. Mater. Synth. Proc.* **1998,** *6*, 49.

(11) Chang, Y.-H.; Chiu, H.-T. *J. Mater. Res.* **2002,** *17*, 2779.

(12) Powder diffraction file card 42-1120. JCPDS: International Center for Diffraction Data, 1601 Park Lane, Swarthmore, PA 19081.

(13) Powder diffraction file card 11-0680. JCPDS: International Center for Diffraction Data, 1601 Park Lane, Swarthmore, PA 19081.

(14) Powder diffraction file card 41-1487. JCPDS: International Center for Diffraction Data, 1601 Park Lane, Swarthmore, PA 19081.

(15) Vix-Guterl, C.; Couzi, M.; Dentzer, J.; Trinquecoste, M.; Delhaes, P. *J. Phys. Chem. B* **2004,** *108*, 19361.
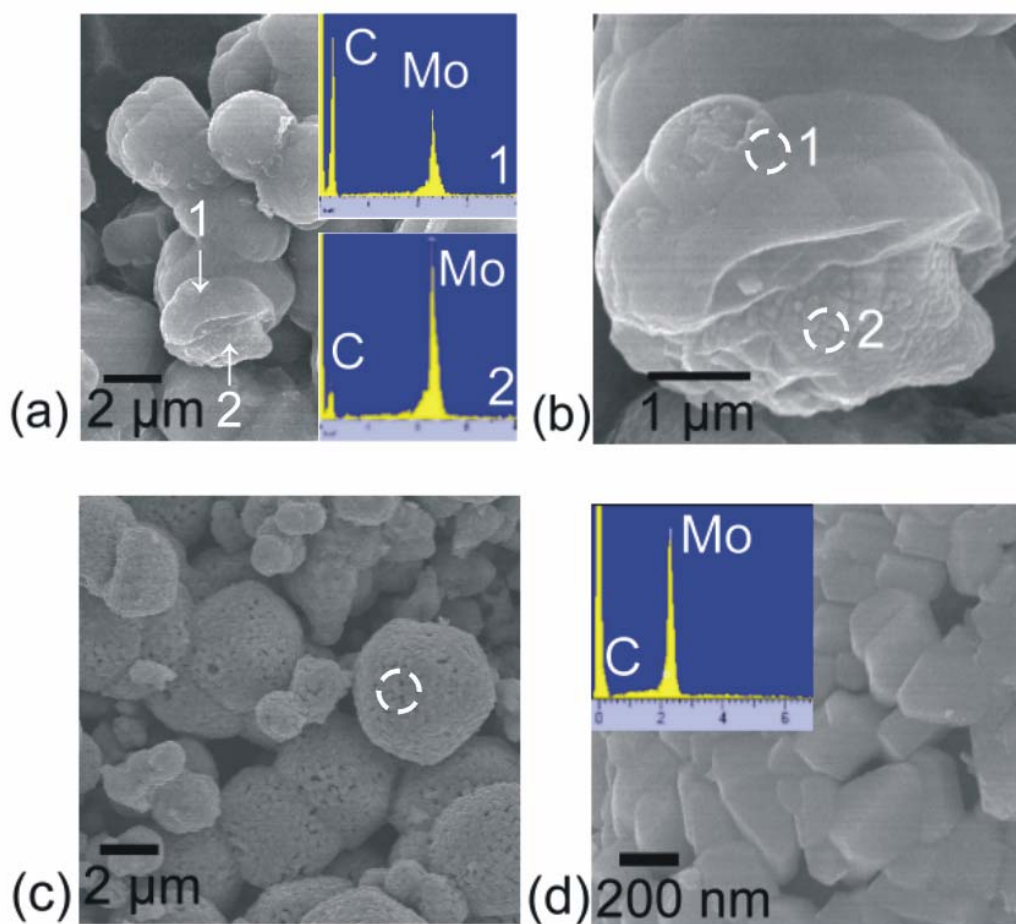
(16) Cotton, F. A.; Wilkinson, G.; Murillo, C.A.; Bochmann, M. in: *Advanced Inorganic Chemistry* (John Wiley & Sons, **1988**) p. 819.
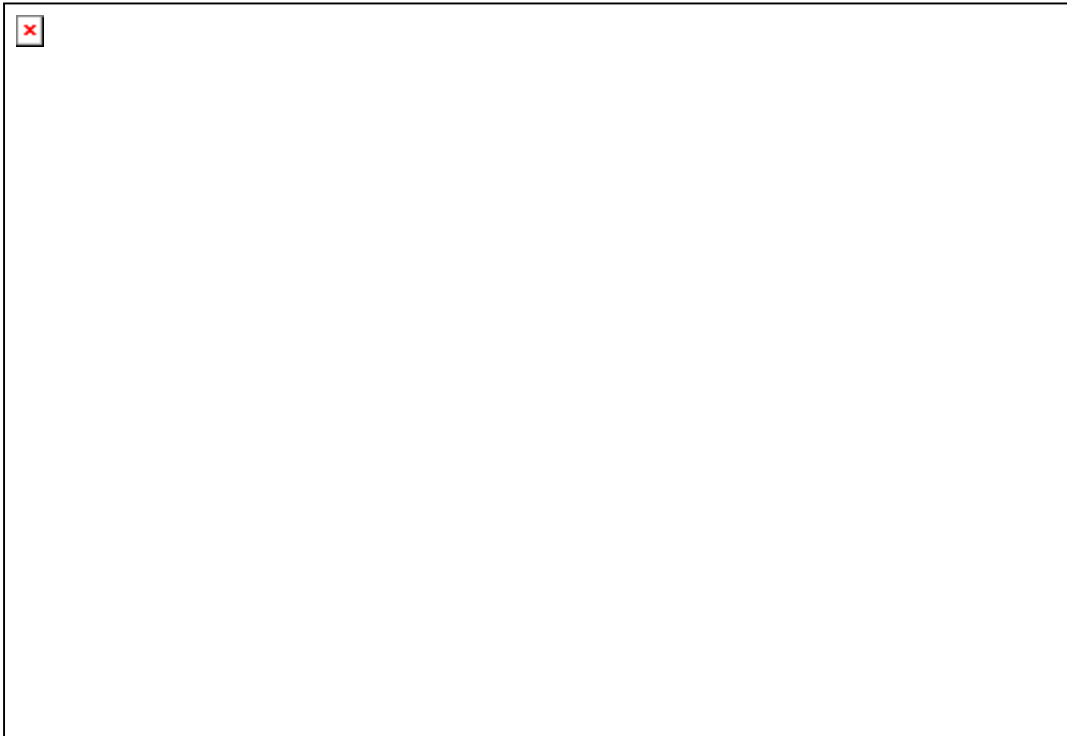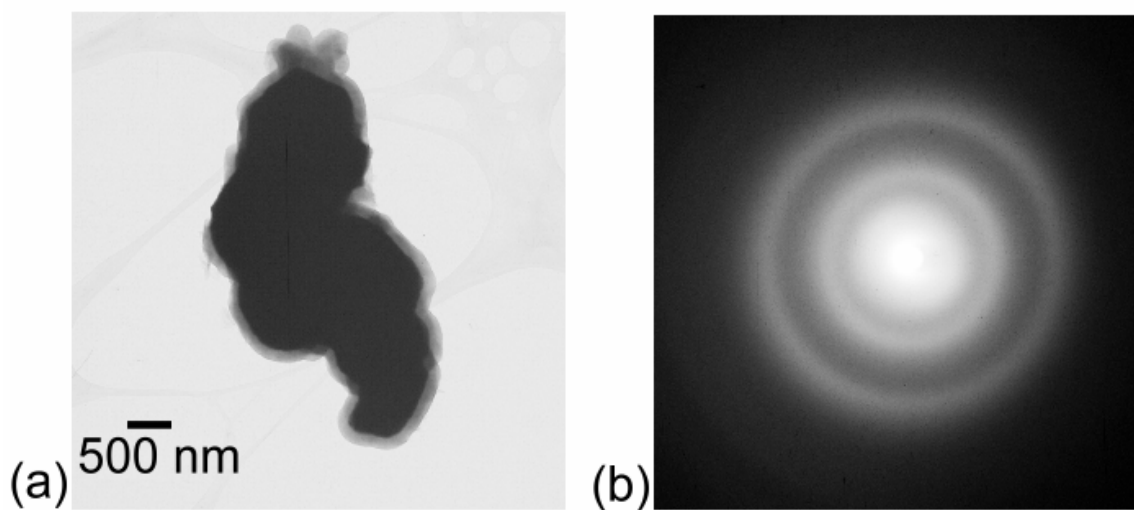
Fig. 5-1 XRD patterns of powders prepared from Mo and 1-chlorobutane at (a) 873 K, (b) 1073 K and (c) 1173 K under a flow of 20 sccm Ar for 8 h. (d) XRD pattern of a powders prepared from Mo and hexachlorobenzene at 1073 K under vacuum for 24 h.
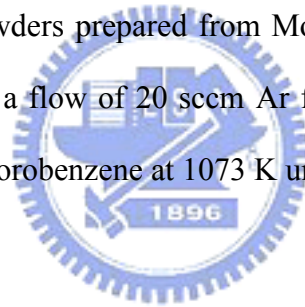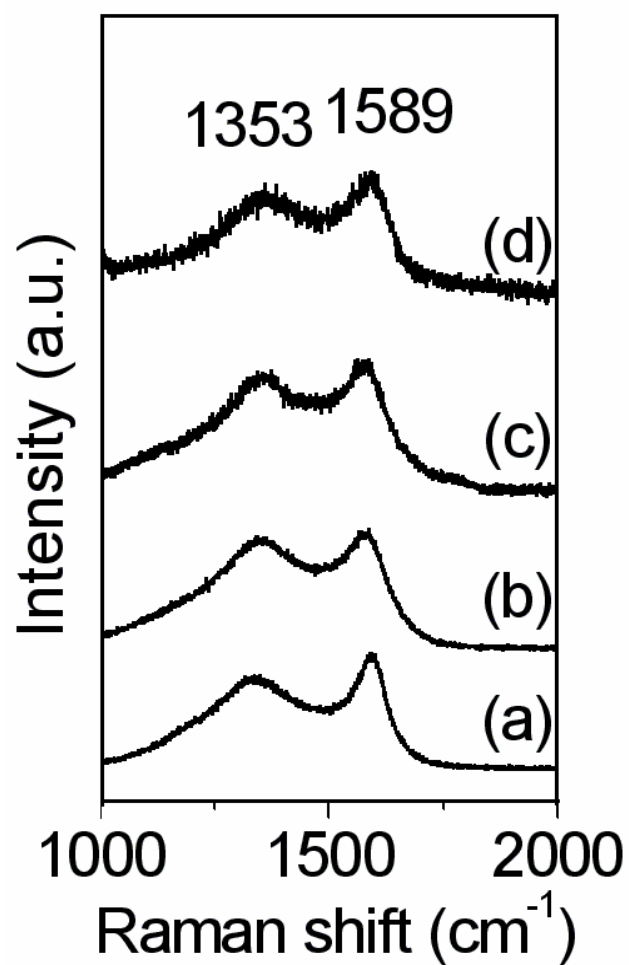
Fig. 5-2 (a) SEM image of a powder prepared from Mo and 1-chlorobutane at 1073 K under a flow of 20 sccm Ar for 8 h; inset: EDS from the spots indicated by arrows **1** and **2**. (b) Enlarged SEM image of the particle shown in (a). (c) and (d) are SEM and EDS (inset) images of a powder prepared from Mo and hexachlorobenzene at 1073 K under vacuum for 24 h.

Fig. 5-3 (a) TEM image of a particle aggregate prepared from Mo and 1-chlorobutane at 1173 K under a flow of 20 sccm Ar for 8 h. (b) ED image of the bottom part of the aggregate shown in (a).

Fig. 5-4 Raman spectra of powders prepared from Mo and 1-chlorobutane at (a) 873 K, (b) 1073 K and (c) 1173 K under a flow of 20 sccm Ar for 8 h. (d) Raman spectrum of a powder prepared from Mo and hexachlorobenzene at 1073 K under vacuum for 24 h.
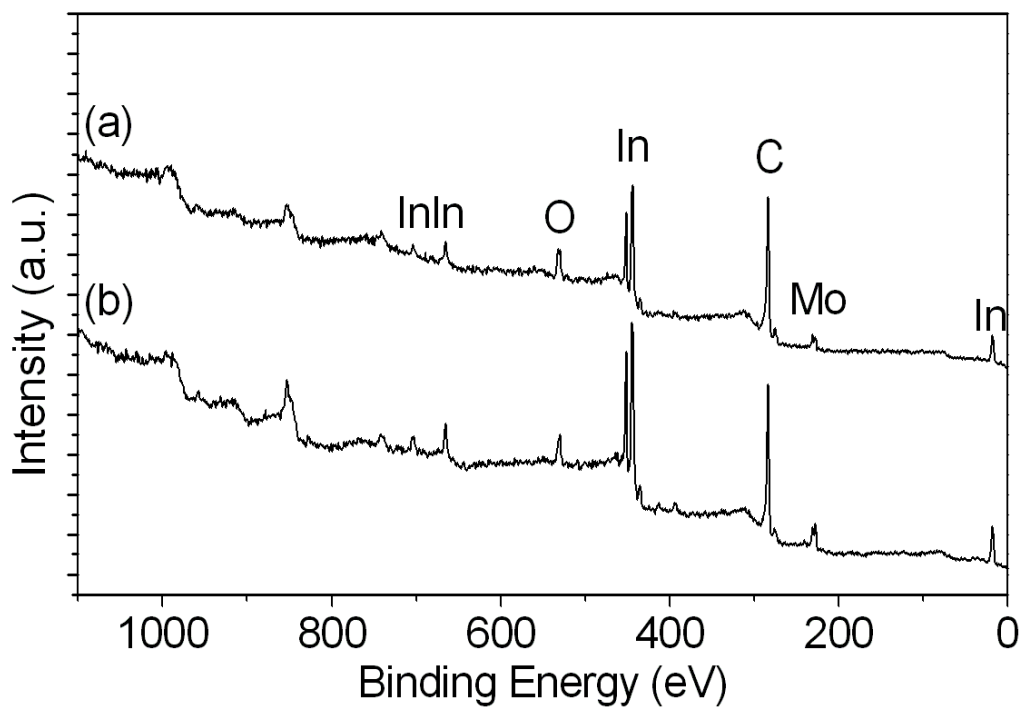
Fig. 5-5 XPS survey of a powder prepared from Mo and 1-chlorobutane at 1173 K under a flow of 20 sccm Ar for 8 h, (a) as-prepared and (b) after Ar$^+$ ion sputtering for 30 s. In metal was used as the sample support.
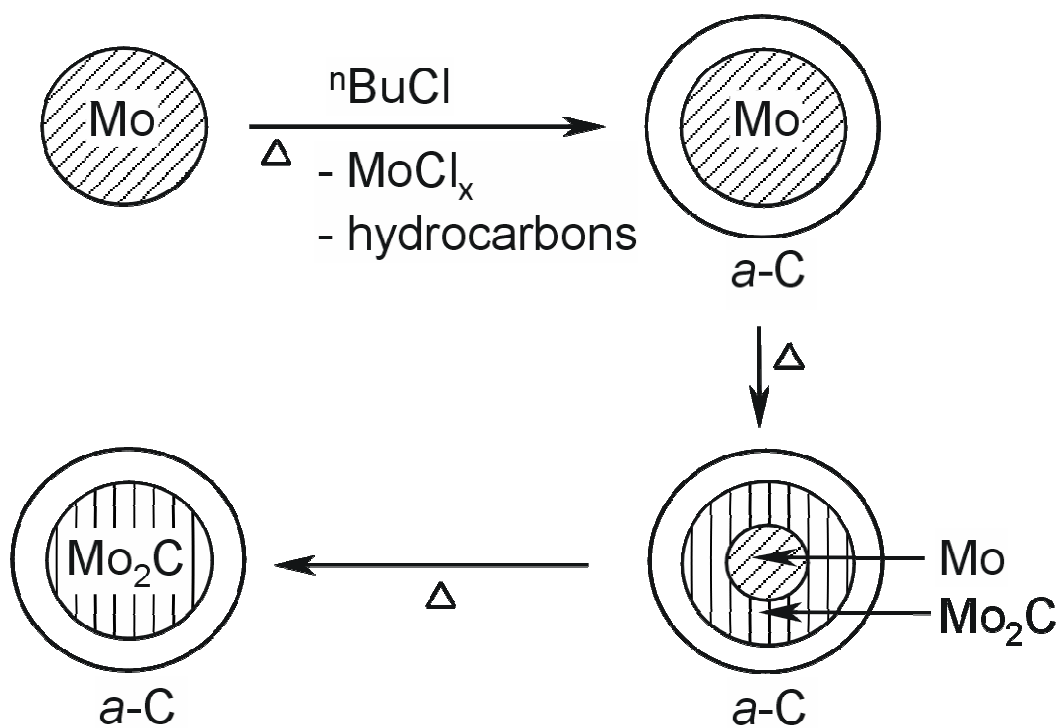
Fig. 5-6 Proposed reaction steps between ^{n}BuCl and Mo to form a $Mo_2C@a$-C particle.
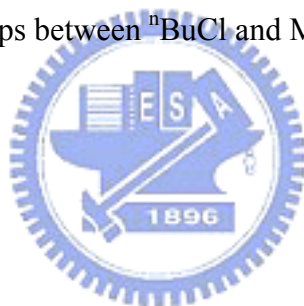
Chapter 6: Template assisted synthesis of carbon particles and hollow shells from CCl_4 and Mo

6.1 Introduction

Carbon hollow spheres and particles have been synthesized by a variety of methods, including direct pyrolysis of hydrocarbons, pyrolysis of hydrocarbons in carbon arc, impregnation and carbonization of organic precursors in mesoporous silica templates, pyrolysis of precursors on monodispersed cobalt nanoparticle template, polymerization of fullerence powders by shock-compression, and chemical vapor deposition (CVD) via mixed-valent oxide-catalytic carbonization (MVOCC) process.[1-11] In addition, recent reports have shown that carbon hollow spheres can be synthesized by reduction of chloroalkanes and alcohols with active metals in autoclave.[12-16] In this chapter, we describe an interesting new reduction reaction process to form carbon hollow spheres by reacting CCl_4 with Mo powders at high temperatures. We report our observations below.

6.2 Experimental Procedure

In typical experiments, Mo powders (1 − 3 μm, Riedel-deHaën) in a quartz boat were placed in a 30 mm diameter quartz tube in a furnace. At 1 atm 873 - 1173 K, CCl_4 (Fisher) at 298 K under a flow of Ar (10 sccm) was bubbled into the reactor for 1 − 4 h to produce black powders.

6.3 Results and Discussion

Fig. 6-1 shows scanning electron microscopic (SEM, JEOL JSM-6330F at 15 kV) and transmission electron microscopic (TEM, Philips TECNAI 20 At 200 kV) images of the powder products. In Fig. 6-1(a), aggregated spherical particles with diameters 1 − 3 μm are

found in the sample prepared at 873 K. The spheres appear to be hollow because some thin shells with thickness ca. 50 nm can also be found in the image. An energy dispersive X-ray spectrum (EDX) of the sample shows that the major component is C while a trace of Cl is also found. A TEM image in Fig. 6-1(b) confirms that the spheres are hollow and the diameter and the layer thickness agree with the SEM observation. An electron diffraction (ED) pattern in Fig. 6-1(b) displays two diffused rings corresponding to (101) and (110) reflections of small graphite crystals.[17] The absence of (002) may be due to that the incident electron beam is perpendicular to local (001) graphite planes.[10] Qian and co-workers also observed the similar phenomenon.[15,16] Fig. 1(c) reveals that the sample prepared at 1073 K consists of carbon spheres. An imperfect sphere exposed that their inner structure is collected nanoparticles with diameters 50 − 100 nm. When the reaction temperature exceeds 1173 K, the SEM and the TEM images in Figs. 6-1(d) and 6-1(e), respectively, suggest that the observed carbon particles have sizes varied between 200 and 300 nm. Few large hollow spheres were found in the product. The ED pattern in Fig. 6-1(e) suggests that the sample contains small crystals. The high-resolution TEM (HRTEM) in Fig. 6-1(f) confirms the presence of laminated layers with short-range orderness, indicating that the carbon particles contain small graphitic fragments. The spacing of the planes is 0.33 − 0.34 nm, close to the interlayer distance of graphite (002) planes, 0.34 nm.[17]

Fig. 6-2 shows the X-ray diffraction (XRD, Bruker D8 Advance, Cu Kα radiation, 40 kV, and 40 mA) patterns of the samples. Fig. 6-2(a) suggests that all of the reactant Mo is consumed and the product prepared from the reaction at 873 K for 4 h is amorphous. Together with the ED pattern in Fig. 6-1(b), we conclude that crystalline domain in the material is only a minor portion. Fig. 6-2(b) displays the XRD of the solid gathered from the reaction at 1073 K for 1 h. The pattern is indexed to a mixture of the reactant Mo and β-Mo_2C, a product from the reaction. When the reaction time exceeds 4 h, the reflections from Mo and β-Mo_2C, as shown in Fig. 6-2(c), become insignificant while the pattern of graphite with broad peak

widths appears. The calculated d-spacing of (002) planes is 0.344 nm, which is slightly larger than the reported value of graphite, d = 0.33756 nm.[17] The XRD data suggest that the degree of long-range orderness in the structure is lower than that of graphite. The result is similar to the observation of other related carbon materials.[12,15,16] For the sample prepared at 1173 K for 1 h, the d-spacing of (002) planes, estimated from the pattern in Fig. 6-2(d), is 03391 nm. This confirms that the particles synthesized at this condition contain graphite.[17]

Raman spectroscopy (Jabin Yvon HR800 quipped with an Ar^+ laser at 514.5 nm) is further used to characterize the carbon products, as shown in Fig. 6-3. Two strong scattering peaks near 1344 and 1579 cm^{-1}, assigned to D and G modes respectively, are observed in the samples prepared at 873 K - 1173 K.[20,21] In some cases, overtones from these vibrations are also observed at 2600 – 3000 cm^{-1}.[20,21] The intensity ratio of D peak to G peak, I_D/I_G, decreases as the reaction temperature increases. This implies that the degree of graphitization is higher for the particles, prepared at 1173 K, than for the carbon hollow shells, synthesized at 873 K. This well agrees with the XRD results.

The reaction pathway between CCl_4 and Mo powders at different temperature is proposed in Scheme 6-1. It is known that CCl_4 decomposes at high temperatures into many dechlorinated species, such as CCl_2, CCl_3, and $CCl_2=CCl_2$.[22] As reported in literature, these species polymerize and dehalogenate further into various carbon containing products.[13,23,24] Thus, we propose that below 873 K, the Mo particle acts as a template for the carbon shell while the inner Mo core is etched away by Cl atoms. At 1073 K, the surface of Mo particle is carbonized initially into a layer of Mo_2C. The overall morphology is preserved in the as-formed composite core/shell particle. As the reaction proceeds, the inner core is also carbonized and etched away. Prolonged reaction probably causes the Mo atoms to be removed completely. This would leave a carbon material with nanoparticles wrapped inside a thin shell. At a high reaction temperature exceeding 1173 K, we expect the reaction rate is fast and the shell structure formation is slower than the etching reaction, which quickly reduces the Mo

particle size. Consequently, the Mo particle does not act as a template at this stage and the reaction generates small graphite particles only.

Calculate the molarity of the carbon shell with thickness 50 nm and the original Mo particle with diameters 1 μm. The densities of graphite (a.w. = 12.01) and Mo (a.w. = 95.94) are 2.16 and 10.22 g/cm^3, respectively.
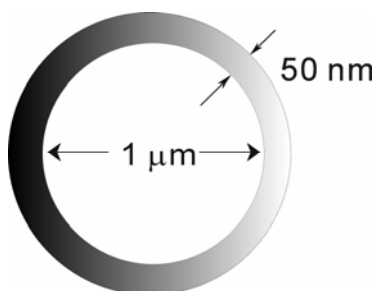
The volume of graphite shell = $1.334 \pi [(1.05 \mu m)^3 - (1 \mu m)^3] = 6.60 \times 10^{-13}$ cm^3

The weight of graphite shell = $(6.60 \times 10^{-13}$ cm$^3) \times 2.16$ g/cm$^3 = 1.425 \times 10^{-12}$ g

No. mol of graphite shell = 1.425×10^{-12} g $\times \dfrac{1 \text{ mol C}}{12.01 \text{ g C}} = 1.186 \times 10^{-13}$ mol

The carbon source is CCl$_4$. Thus,

No. mol of Cl = $4 \times (1.186 \times 10^{-13}) = 4.744 \times 10^{-13}$ mol

The volume of original Mo particle = $1.334 \pi (1 \mu m)^3 = 4.849 \times 10^{-12}$ cm^3

The weight of original Mo particle = 4.849×10^{-12} cm$^3 \times 10.22$ g/cm$^3 = 4.956 \times 10^{-11}$ g

No. mol of original Mo particle = 4.956×10^{-11} g $\times \dfrac{1 \text{ mol Mo}}{95.94 \text{ g}} = 5.165 \times 10^{-13}$ mol

The mole ratio of Cl to Mo = $\dfrac{4.744 \times 10^{-13} \text{ mol}}{5.165 \times 10^{-13} \text{ mol}} = 0.9196$

The mole ratio of Cl to Mo indicates the carbon shell provided insufficient Cl atoms for removing the original Mo particle. The other Cl atoms should be supplied by the decomposition of CCl$_4$ in the gas phase. The pyrolysis and polymerization of the dechlorinated species induced the formation of the carbon shells.

6.4 Conclusions

In conclusion, carbon hollow spheres (1 – 3 μm) and particles (200 – 300 nm) have been synthesized from CCl_4 and Mo at 873 K - 1173 K. The reaction is a combination of pyrolysis, polymerization, dechlorination and etching processes of the reactants. The morphology of the carbon products is highly affected by the reaction temperature and the Mo morphology.

6.5 References

(1) Krishnan, A.; Dujardin, E.; Treacy, M.M.J.; Hugdahl, J.; Lynum, S.; Ebbesen, T. W. *Nature* **1997,** *388*, 451.

(2) Su, F.; Zeng, J.; Yu, Y.; Lv, L.; Lee, J.Y.; Zhao, X.S. *Carbon* **2005,** *43*, 2366.

(3) Xia, Y.D.; Mokaya, R. *Adv. Mater.* **2004,** *16*, 886.

(4) Oda, Y.; Fukuyama, K.; Nishikawa, K.; Namba, S.; Yoshitake, H.; Tatsumi, T. *Chem. Mater.* **2004,** *16*, 3860.

(5) Tosheva, L.; Parmentier, J.; Valtchev, V.; Vix-Guterl, C.; Patarin, J. *Carbon* **2005,** *43*, 2474.

(6) Niwase, K.; Homae, T.; Nakamura, K.G.; Kondo, K. *Chem. Phys. Lett.* **2002,** *362*, 47.

(7) Jin, Y. Z.; Gao, C.; Hsu, W. K.; Zhu, Y.; Huczko, A.; Bystrzejewski, M.; Roe, M.; Lee, C. Y.; Acquah, S.; Kroto, H.; Walton, D. R.M.. *Carbon* **2005,** *43*, 1944.

(8) Jin, Y. Z.; Kim, Y. J.; Gao, C.; Zhu, Y. Q.; Huczko, A.; Endo, M.; Kroto, H. W. *Carbon* **2006,** *44*, 724.

(9) Serp, Ph.; Feurer, R.; Kalck, Ph.; Kihn, Y.; Faria, J.L.; Figueiredo, J.L. *Carbon* **2001,** *39*, 615.

(10) Wang, Z.L.; Yin, J.S. *Chem. Phys. Lett.* **1998,** *289*, 189.

(11) Lu, A.-H.; Li, W.-C.; Matoussevitch, N.; Spliethoff, B.; Bönnemann, H.; Schüth, F. *Chem. Commun.* **2005,** 98.

(12) Liu, J.W.; Shao, M.W.; Tang, Q.; Chen, X.Y.; Liu, Z.P.; Qian, Y.T. *Carbon* **2002,** *41*, 1645.

(13) Xiong, Y.; Xie, Y.; Li, Z.Q.; Wu, C.Z.; Zhang, R. *Chem. Commun.* **2003,** 904.

(14) Hu, G.; Ma, D.; Cheng, M.; Liu, L.; Bao, X. *Chem. Commun.* **2002,** 1948.

(15) Shi, L.A.; Gu, Y.; Chen, L.Y.; Yang, Z.H.; Ma, J.H.; Qian, Y.T. *Chem. Lett.* **2004,** *33*, 532.

(16) Zhang, W.; Liu, J.W.; Huang, Z.; Ma, D.K.; Liang, J.B.; Qian, Y.T. *Chem. Lett.* **2004,** *33*,

1346.

(17) Powder diffraction file card 41-1487. JCPDS: International Center for Diffraction Data, 1601 Park Lane, Swarthmore, PA 19081.

(18) Powder diffraction file card 42-1120. JCPDS: International Center for Diffraction Data, 1601 Park Lane, Swarthmore, PA 19081.

(19) Powder diffraction file card 11-0680. JCPDS: International Center for Diffraction Data, 1601 Park Lane, Swarthmore, PA 19081.

(20) Liu, J.W.; Shao, M.W.; Chen, X.Y.; Yu, W.C.; Liu, X.M.; Qian, Y.T. *J. Am. Chem. Soc.* **2003,** *125***,** 8088.

(21) Hou, H.Q.; Schaper, A.K.; Jun, Z.; Weller, F.; Greiner, A. *Chem. Mater.* **2003,** *15*, 580.

(22) Swift, F.; Sung, R.L.; Doyle, J.; Stille, J.K. *J. Org. Chem.* **1965,** *30*, 3114.

(23) Wu, Y.-P.; Won Y.-S. *Combust. Flame* **2000,** *122*, 312.

(24) Reaction-Web, Facility for the Analysis of Chemical Thermodynamics, CRCT, École Polytechnique de Montre´al: Montre´al, http://www.crct.polymtl.ca/fact/.
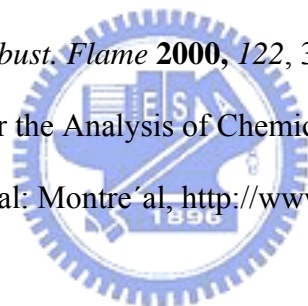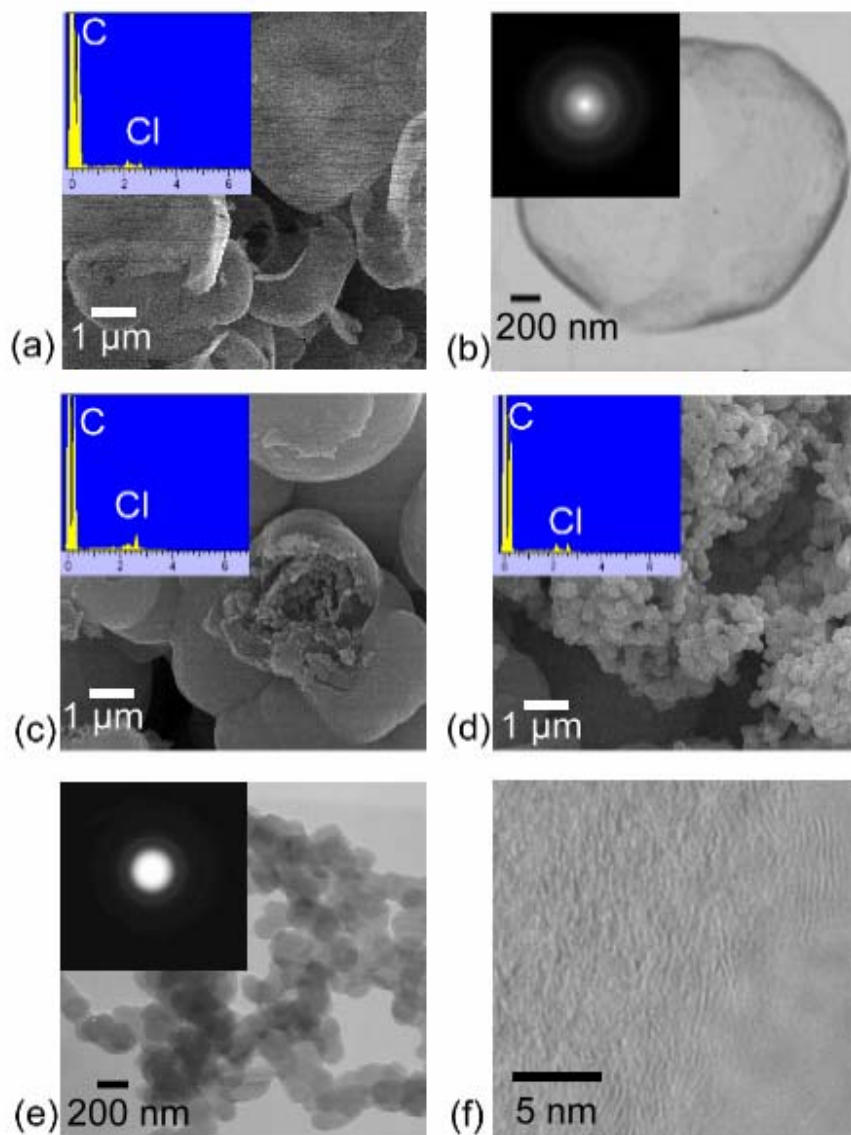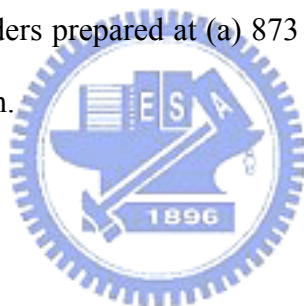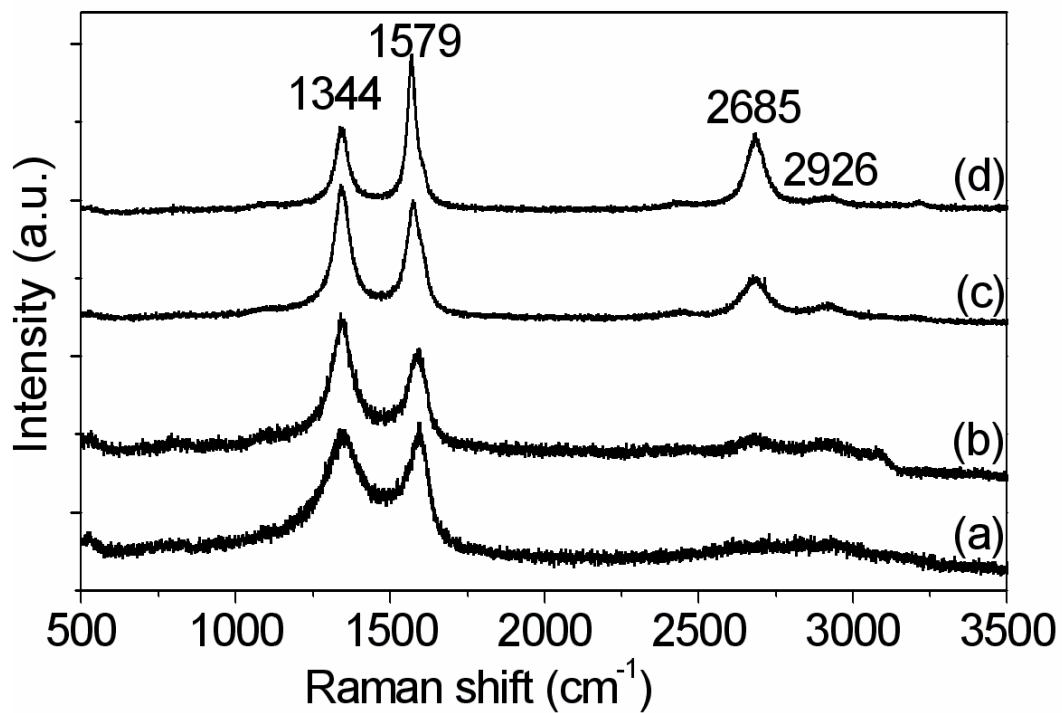
Fig. 6-1 (a) SEM and EDS (inset) images of powders prepared at 873 K for 4 h. (b) TEM and ED (inset) images in (a). (c) SEM and EDS (inset) images at 1073 K for 4 h. (d) SEM and EDS (inset) images of powders prepared at 1173 K for 1 h. (e) TEM and ED (inset) images in (d). (f) HRTEM images in (d).
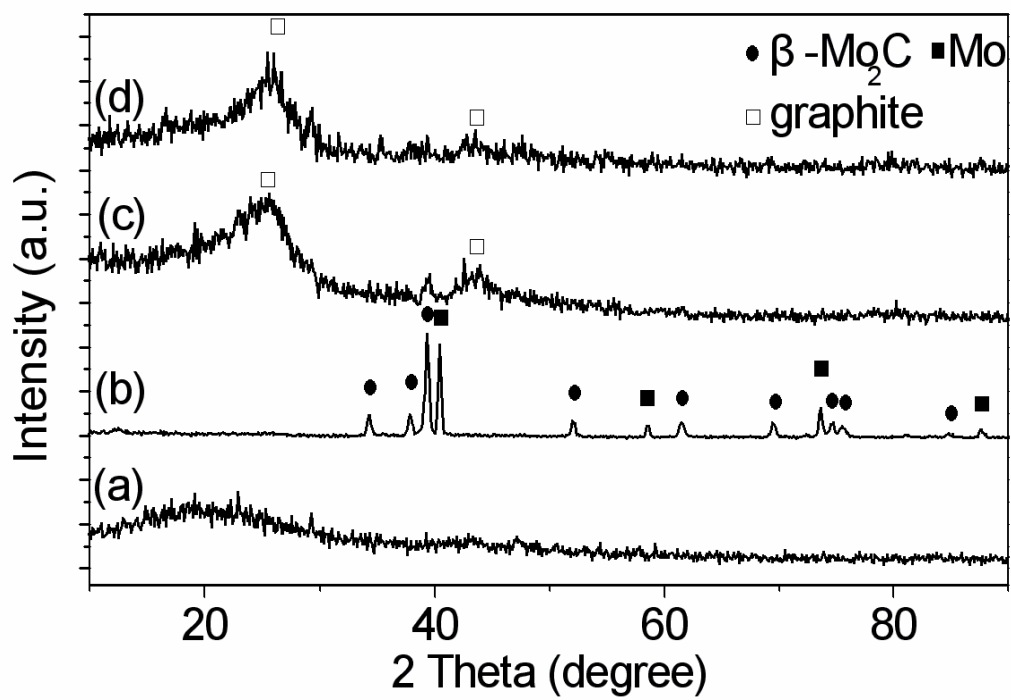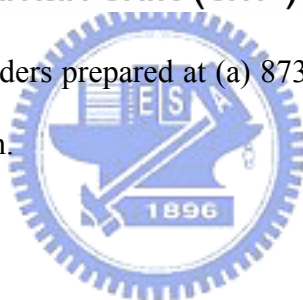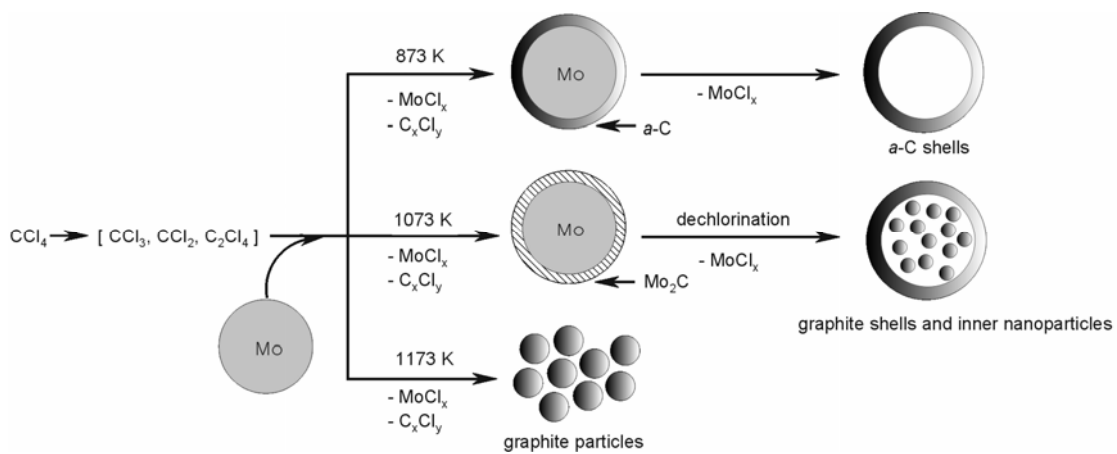
Fig. 6-2 XRD patterns of powders prepared at (a) 873 K for 4 h, (b) 1073 K for 1h, (c) 1073 K for 4 h and (d) 1173 K for 1 h.

Fig. 6-3 Raman spectra of powders prepared at (a) 873 K for 4 h, (b) 973 K for 4 h, (c) 1073 K for 4 h and (d) 1173 K for 1 h.
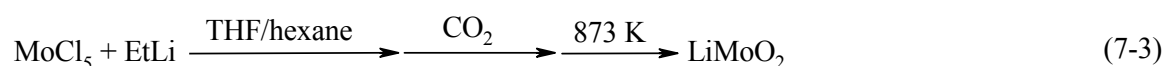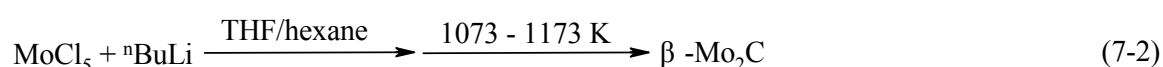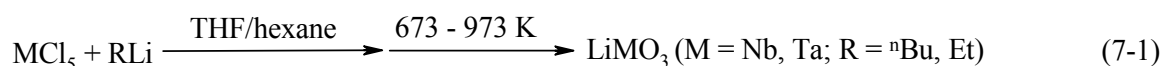
Scheme 6-1 Proposed reaction pathway.

Chapter 7: Summary

In this thesis, we employ two synthetic routes, including liquid-phase processing and gas-solid reactions, to prepare carbides and lithiated oxides of group V and VI metals. The liquid-phase routes are shown below:

$$MCl_5 + RLi \xrightarrow{\text{THF/hexane}} \xrightarrow{673 - 973 \text{ K}} LiMO_3 \text{ (M = Nb, Ta; R = }^nBu, Et)} \qquad (7\text{-}1)$$

$$MoCl_5 + {}^nBuLi \xrightarrow{\text{THF/hexane}} \xrightarrow{1073 - 1173 \text{ K}} \beta\text{-}Mo_2C \qquad (7\text{-}2)$$

$$MoCl_5 + EtLi \xrightarrow{\text{THF/hexane}} \xrightarrow{CO_2} \xrightarrow{873 \text{ K}} LiMoO_2 \qquad (7\text{-}3)$$

In our previous report, the reactions between the metal chlorides of group V and n-butyllithium in hexane generated the precursors for the metal carbides. When THF was used as the second solvent in the reaction, alkyllithium was changed to lithium enolate. The reactions between the metal chloride of group V and lithium enolate, shown in Eq. (7-1), produced the polymeric $[LiM(OR)_m]_n$ precursors for lithiated metal oxides. Nanosized $LiTaO_3$ (50 – 100 nm) and $LiNbO_3$ (20 – 50 nm) powders can be obtained by annealing the polymeric precursors. The M-O bond formation after a metathetic reaction between M-Cl and Li-OR bonds at molecular level in the precursors leads to the ultimate formation of $LiTaO_3$ and $LiNbO_3$ at low temperatures.

But similar results are not observed in the reaction between molybdenum chloride and n-butyllithium in a mixed solvent contained THF and hexane. Although $MoOCl_3(THF)_2$ was formed by reacting $MoCl_5$ with THF at first, molybdenum carbides were synthesized by annealing the precursor created by the reaction between $MoOCl_3(THF)_2$ and n-butyllithium as shown in Eq. (7-2) is well illustrated. We expect that all elements are intermixed in the precursor at molecular level. When the precursor is decomposed at high temperature, excess O atoms probably were removed by C atoms via carbothermal reduction steps. Nanosized

Mo_2C (10 – 30 nm) was obtained at last.

Amazingly, $LiMoO_2$ was synthesized from a precursor prepared by reacting EtLi and $MoCl_5$ in THF followed by a long time oxidation. The Eq. (7-3) shows this novel route. We speculate that $LiMoO_2$ was synthesized by the reaction between molybdenum oxides and Li_2CO_3 formed from CO_2 in the air.

Eqs. (7-4), (7-5) and (7-6) show the gas-solid reactions between Mo powders and chlorinated reactants. Three reactants with different ratios of chlorine to carbon, include 1-chlorobutane, hexachlorobenzene and carbon tetrachloride, were selected as the gas reagents. From the result, the chlorine ratios of the gas reagent affected the morphology of the products apparently. 1-Chlorobutane not only acted as the carbon source to carbonize Mo powders but also covered the surface to form the core/shell structure. Hexachlorobenzene provided more chlorine atoms to etch the metal into smaller particles. The carbon tetrachloride, the highest ratio of chlorine to carbon in organic compound, exhausted all molybdenum powders and formed the graphite shells. The reaction between carbon tetrachloride and Mo powders is a combination of pyrolysis, polymerization, dechlorination and etching processes of the reactants.

$$Mo + {}^nBuCl \xrightarrow{\text{873 - 1173 K}} Mo_2C@a\text{-C particles} \tag{7-4}$$

$$Mo + C_6Cl_6 \xrightarrow{\text{1073 K}} Mo_2C \text{ nanoparticles} \tag{7-5}$$

$$Mo + CCl_4 \xrightarrow{\text{873 - 1173 K}} \text{carbon particles and hollow shells} \tag{7-6}$$